The mid-to-late Holocene water level and climate changes of Lake Salda (SW Anatolia/Turkey): Evidence from high-resolution seismic and sediment core records

Asen Sabuncu (sabuncuas@itu.edu.tr)
Eurasia Institute of Earth Science, Istanbul Technical University, Ayazağa, 34469 İstanbul, Turkey

Kürşad Kadir Eriş
Faculty of Mines, EMCOL Applied Research Center, Department of Geological Engineering, Istanbul Technical University–Ayazaga Campus, Istanbul, Turkey

Gülsen Uçarkuş
Faculty of Mines, EMCOL Applied Research Center, Department of Geological Engineering, Istanbul Technical University–Ayazaga Campus, Istanbul, Turkey

Dursun Acar
Faculty of Mines, EMCOL Applied Research Center, Department of Geological Engineering, Istanbul Technical University–Ayazaga Campus, Istanbul, Turkey

Erdem Kırkan
Faculty of Mines, EMCOL Applied Research Center, Department of Geological Engineering, Istanbul Technical University–Ayazaga Campus, Istanbul, Turkey

Nurettin Yakupoğlu
Faculty of Mines, EMCOL Applied Research Center, Department of Geological Engineering, Istanbul Technical University–Ayazaga Campus, Istanbul, Turkey

Sena Akçer Ön
Muğla Sıtkı Koçman University

Nurgul Balcı
Department of Geological Engineering, Istanbul Technical University–Ayazaga Campus, Istanbul, Turkey

---

Research Article

Keywords: Lake Salda, Holocene, lake-level, sediment core, seismic stratigraphy

Posted Date: September 8th, 2022

DOI: https://doi.org/10.21203/rs.3.rs-2021930/v1

Abstract

The sedimentary sequence in Lake Salda has been first documented in detail by analyses of high-resolution seismic profiles and sediment cores together with onshore outcrops along the present coastline of the lake. Such a multi-proxy approach provides a sensitive record of changing lake level and depositional conditions in Lake Salda during the mid-to-late Holocene. The low water level during the middle Holocene is followed by subsequent lake level decrease until 1690 cal year BP due to a drier climate. This prominent climate deterioration induced the coastal regression in the lake as inferred from the progradational deltaic sequences in the high-resolution seismic record. During the same period of a dry climate, oligotrophic lake conditions gave rise to the formation of stromatolite in the lake, timely coinciding with the Roman Warm Period. The following period of the late Holocene is represented by considerable lake level drop due to the enhanced dry climate that is earmarked by prominent erosional truncation surface and channel-incisions in the seismic profiles. This aridification phase is subsequently followed by transgressive lake level during 1690-1050 cal year BP, giving rise to a retreat of the deltaic deposit further inland as documented in the high-resolution seismic profile. The further deepening of the lake by contributions of both climate and tectonics during the last 650 cal year BP produced a transgressive unit with typical of onlapping architecture in the seismic reflection profiles and the formation of Gilbert-type fan deltas along the shoreline.

Highlights

- Definition and timing of depositional units based on seismic and core correlations.
- Water level reconstruction in Lake Salda during the last ~4,200 cal year BP.
- Interaction of clastic system with local climate and lake level.

Introduction

Lakes are dynamic response systems that incorporate environmental, climatic, and tectonic forcing into a continuous, high-resolution archive of local and regional change. The interaction among them can be documented by seismic stratigraphic analysis of lake sediments that in turn allow us to examine past water-level variability. On the other hand, sediment coring in lakes provides the history of undisturbed sedimentary sequence that is needed to be calibrated by high-resolution reflection seismic profiling in order to obtain a robust chronology of sedimentary units deposited across the entire lacustrine sedimentary system. For this purpose, an accurate depth correction of sediment core to seismic reflection profiles is vital, which could be produced by synthetic seismograms calculated from the physical properties of sediment cores.

Valuable information on regional and global scale patterns of past climate variability in the Mediterranean region has been documented by numerous paleoclimate studies (Bar-Matthews et al. 2000; Jones et al. 2006; Tzedakis, 2007; Kotthoff et al. 2008; Schmiedl et al. 2010), but some of these may partly explain the contradictory palaeoclimate histories. However, although the Holocene past

climate variability in eastern and middle Anatolia has been extensively documented by numerous lake core studies (Kempe et al. 2002; Wick et al. 2003; Jones et al. 2006; Çağatay et al. 2014; Leroy et al. 2002, 2009, 2010; Eriş et al. 2018; Ön et al. 2018; Ocakoğlu et al. 2019), there are still ambiguities on the timing and intensity of specific climate periods due to geographical variation across the overall Anatolia during the mid-to-late Holocene, resulting in difficulties in correlating different lake records. The perennial Lake Salda is a unique setting for paleoclimate and paleoenvironmental studies due to Mg-rich alkaline waters, living stromatolites and sedimentary biomarkers. Although the paleoclimate change for the latest Holocene period in Lake Salda has been recently documented (Danladi and Ön, 2018), the interaction of lake level change and depositional settings is still unknown. In this study, the analyses of the sedimentary record of Lake Salda provide a detailed record of the lake level fluctuations, thus allowing us to establish a complete picture of the climate condition in western Anatolia during the mid-to-late Holocene.

This study is the first attempt to establish the seismostratigraphic analysis of the depositional units by using core-to-seismic correlation that enables us to examine the extent of various sedimentary seismic facies and reconstruct past lake level changes during the mid-to-late Holocene. Correlation of seismic stratigraphic units calibrated by ^{14}C-dated sedimentary units in the studied cores and facies analysis of outcrops along the present coastline of the lake document a robust chronostratigraphic framework of the depositional units deposited under fluctuating water level and climate around Lake Salda.

Regional Settings

Lake Salda is located NW of the Yeşilova province (Burdur/Turkey) in SW of Anatolia (Fig. 1). It occupied a depression at an altitude of 1180 m above sea level and was surrounded by Doğanbaba and Eseler Mountain in the Taurus tectonic belt with 8.2 km length and 6.4 km wide (Kocaefe and Ataman, 1976) (Fig. 1b). Lake Salda has a surface area of 43.7 km^2 with a maximum depth of ~186 m (Kazancı et al. 2004), which is covered by mainly consist of Quaternary alluvial unit, Cretaceous ultramafic rocks and Middle Triassic/Lias limestone Sarp 1976; Çaldırak et al. 2017). The Quaternary sediment wedge constituting the coastal plain overlies the Cretaceous ultramafic rocks and Middle Triassic/Lias limestone. The bedrock in the western catchment area of Lake Salda consists of Pliocene-aged sandstone, claystone, marl, clayey limestone and conglomerate rocks (Senel et al. 1989).

The entire perimeter of the lake is covered by hydromagnesite stromatolites, occurring through microbial reactions (Braithwaite and Zedef 1996; Zedef et al. 2000; Kaiser et al. 2016; Balcı et al. 2020). Assorted studies were carried out on the present limnology (Braithwaite and Zedef 1996; Kazancı et al. 2000, 2004) and the water chemistry of Lake Salda (Kazancı et al. 2004; Shirokova et al. 2011, 2013; Mavromatis et al. 2015; Kaiser et al. 2016). In addition, the similarity of Jezero Crater on Mars (Salvatore et al. 2018) interests researchers in investigating Mg-carbonate deposits in Lake Salda along the present shoreline (Horgan et al. 2020). Recently, Balcı et al. (2020) presented chemical and biological factors controlling lake water chemistry to provide a better understanding of the limnological properties and biological productivity in the lake. In addition, some other studies documented the tectonic structure of the surrounding (Schmidt 1987; Braithwaite and Zedef 1994, 1996; Russell et al. 1999; Zedef et al. 2000;

Kazancı et al. 2004) the evaluation of climate and human effects on the lake region (Danladi and Ön 2018; Davraz et al. 2019; Dereli and Tercan 2020). Lake Salda has alkaline water chemistry with a pH of 9.1 and salinity of 1.3 g per liter. The regional climate around Lake Salda is influenced by the Mediterranean climate to the south and the continental Anatolian climate to the north. Average temperatures range from 2.6 °C in January to 24.7 °C in July. The precipitation is highest in winter and is strongly controlled by the local morphology. Annual precipitation is measured from the lowlands of the Salda valley and the surrounding mountains, ranging from 750 mm to higher than 1200 mm (Turkish State Meteorological Service, 2015). In addition, a few current groundwater inflows provide fresh water to the lake (Balcı et al. 2018).

Materials And Methods

High-resolution seismic reflection data

High-resolution seismic (HR) data of Lake Salda were acquired in 2014 and 2019 with Innomar SES2000 compact system mounted on the side of the coring platform (Fig. 1b). During the survey, signals are penetrated ~ 30 m below lake floor with an optimum frequency range between 2.75 to 6.75 kHz, centered at 3.5 kHz and 40 dB gain level. Sound velocity was converted from time to depth using 1550 ms^{-1} in the water column. The data from the sub-bottom profilers and the navigation system were recorded in XTF format. The HR data of 75 km length was analyzed using the scripts on MATLAB programming language consisting of XTF-SEGY convert, delay-time correction, gain recovery, amplitude scaling, amplitude envelope calculations and interpreted with IHS Kingdom Suite based on 2D Hunt amplitude difference tracing module. The seismic stratigraphic interpretation was performed by using KINGDOM Suite (2018 version) and was based on the identification of unconformity- or conformity-bounded seismic units characterized by distinctive seismic facies.

Sediment cores

The studied sediment cores were retrieved on a portable platform during two different field excursions in Lake Salda during 2014 and 2019 (Fig. 1b). A piston core Salda2014-P02 (3.62 m.) was previously examined and described by Ön et al. (2017), whereas an additional gravity core Salda-2 (1.41 m) has been analyzed in this study (Fig. 1b; Table 1). Split core halves were analyzed in the Core Analyses Laboratory of the Eastern Mediterranean Centre for Oceanography and Limnology (ITU-EMCOL) in İstanbul Technical University. Following detailed lithological descriptions, all halves were used for the Multi-Sensor Core Logger (MSCL) analyses and radiocarbon sampling.

Table 1
Studied cores on Lake Salda (mblf, meters below lake floor)

Core	Site	Water Depth (m)	Core Length (m)	Survey Year	Latitude (N)	Longitude (E)
Salda2014-P02	Western shelf	-29.00.	3.55.	2014	37.54824	29.66210
Salda-02	Western shelf	-13.50	1.35.	2019	37.53305	29.66963

Multi-Sensor core logger (MSCL)

The physical properties (gamma density, P-wave velocity and magnetic susceptibility) of the sediment cores were performed by GEOTEK Multi-Sensor Core Logger (MSCL) in the EMCOL. The split-half piston cores were logged for MSCL physical properties at 1 cm resolution in the ITU EMCOL's Core Analysis Laboratory. Standard calibration and logging methods described by Weaver and Schultheiss (1990) were applied for the MSCL analysis. P-wave velocities and Gamma-ray density is calculated from measured p-wave travel time in the halve of the sediment core within counted protons, respectively. The MSCL analysis of core Salda2014-P02 was previously reported by Ön et al. (2017), whereas core Salda-2 was first analyzed and examined in this study.

Synthetic seismogram and WLS modeling

During HR seismic acquisition survey, Hilbert Transform is used on the accomplished signals to eliminate the undesired amplitudes on different sedimentary zones on acquisition. With this transformation in the processing step, the oscillating parts of the data were missed in both positive amplitude levels. Hence, synthetic seismograms are generated from the calculated reflection coefficients for each sampling interval using density and P-wave velocity values with Klauder wavelet with a zero-phase embedded from auto-correlated Chirp signal are used to acquire these oscillations accurately (Eq. 3.1). The estimated Klauder wavelet with ultimate frequency (f) derivate from the time (t) variables is calculated from Eq. (3.1). In this order, the sampling rate is 1.10^{-5} with 0.01 sec. signal long including with 2–7 kHz bandwidth.

$$s(t) = \cos\left[2\pi\left(f_1 t + \frac{(f_2 - f_1)}{2T} * t^2\right)\right] \quad \text{Eq. (3.1)}$$

To reduce the side oscillations and increase the resolution of the Klauder wavelet, frequency domain spike deconvolution was performed using Eq. (3.2), besides the ε parameter is taken as %1 in this study.

These entire domain transformations, convolution and amplitude corrections on sediment cores are applied in the MATLAB programming language.

$$K^{-1}(\omega) = {K(w)}\Big/{|K(w)| + \varepsilon.max|K(w)|} \qquad \text{Eq (3.2)}$$

One of the main prominences in this study is to set up the chronostratigraphy based on HR seismic reflection profiles with generated synthetic seismograms within the time domain. White (1980) discussed filtered synthetic traces via the goodness-of-fit of the least-squares to detect a coherent (signal) to incoherent (noise) ratio. Thus, a 2D layered model with Weighted-Least Squares (WLS) analyses on two sediment cores was applied to calculate the desired relevant acoustic properties to get more determinable boundaries. On acoustic properties in which are expressed as the P-wave velocity, bulk density and magnetic susceptibility from MSCL analysis according to the general formula:

$$\left[\left(w(x,z_i)\frac{dzi+1}{dx}\cdots 1\vdots\ddots\vdots\mu\frac{d^2zi+1}{dx^2}\cdots zi\right)\right] \approx \left[p\,(x,zi)\,11\vdots w\,(x,zi)\vdots 11ms(x,zi)\right] \text{ Eq. (3.3)}$$

In this iterative scheme of computing the horizon *zi + 1(x)* at the *i*th iteration, used weights as *W(x,zi)* and *p,w,ms* present the density and interval velocity on the previously updated amplitude. Alliterative modeling and their modifications were calculated on MATLAB used with "*nlinfit*" function.

Bathymetry and topographic interpolations

Over ~ 70 km of seismic lines enable us to image the subsurface of the lake with a dense grid of five north to south lines, six east to west lines and some additional lines in selected areas (Fig. 1b). Spline interpolation and triangular irregular network (TIN) methodology with overall was applied to generate a bathymetric map using the mblf points reached from HR seismic dataset. Furthermore, 300-DEM of the Shuttle Radar Topography Mission (SRTM3) dataset was used and interpreted to generate topography from multispectral images of the region and the present shoreline (Dereli et al. 2020). These interpolations were applied by Global Mapper v20 mapping software.

Radiocarbon dating and age-depth modeling

The AMS (accelerator mass spectrometry) radiocarbon dating from two samples of pollen fossils were analyzed for radiocarbon dating in the TÜBİTAK-MAM AMS laboratory (Table 2). Except for the radiocarbon datings, a prominent tephra layer in core Salda2014-P02 has been previously defined and dated by Ön et al. (2017), giving an age of ca. 3560 ± 15 years BP. All ages in core Salda-2 were calibrated with the *"intcal20"* calibration curve (Reimer et al. 2020). Calibrated ages were processed on a statistical development environment named R-Studio using the "Clam" script, based on non-bayesian statistics to obtain an age-depth model for the core's sedimentary units (Blaauw 2010). A Clam module depending on

a linear age-depth model with the estimation of the error rates on the core is specified, and a more realistic model is constructed.

Table 2
Radiocarbon ages obtained for studied cores and peat sample.

Dated Fossil (lab. Number)	Core / Location	Unit	Core (Depth)	Radiocarbon Age (years BP)	Calibrated Radiocarbon Age (years BP)
Pollen	Salda-2	Unit S-1	57–59 cm	920 ± 25	847 ± 25
Pollen	Salda-2	Unit S-2	132–134 cm	1890 ± 25	1792 ± 15
Tephra Layer	SALDA2014-P02	Unit S-3	302 cm.	3560 ± 15	
Peat	L1			700 ± 55	

Results

Seismic stratigraphy

The seismic stratigraphy of sedimentary infill in Lake Salda has been examined by 14 high resolution (HR) seismic profiles with the NW-SE orientated grid (Fig. 1b). In the HR seismic profiles, four seismic units (S4 to S1 from the bottom upward) are bounded by three main reflector surfaces below the lake floor (reflectors SR-1 to 3) (Figs. 2–4). Only seismic units S1, S2 and S3 can be widely traced in the seismic profiles and penetrated by the sediment cores, whereas the deeper unit S4 does not provide a continuous record in all studied profiles. The overall succession of sediments observed in the HR seismic profiles begins in the base section with unit S4 (Figs. 2–4). It extends towards the inner shelf to a water depth of at least 12 m, and has an apparent thickness ranging from 1 to 4 m. On the inner shelf, unit S4 contains acoustically moderate to transparent internal reflectors in seismic profile SLD-01, reflecting slightly inclined clinoforms (Figs. 2b and 3a). The same unit also appears as highly reflective conformable parallel beds on the deeper site of the lake (Fig. 2c). In the HR seismic profiles, unit S4 is overlain by unit S3, the two being separated by the erosional reflection surface SR-3, truncating the internal reflectors of the underlying unit (Figs. 2a, 2b and 3a). The same reflection surface SR-3 in seismic profile SLD-11 is traced as an undulatory surface, extending down upto − 40 m (Fig. 3b).

In the HR seismic profiles, unit S3 is penetrated by core Salda2014-P02 on the inner shelf (Fig. 2a), whereas the same unit basinward in the lake is recorded at the base of core Salda-2 (Fig. 4). This unit

(S3) indicates different facies associations based on various reflection configurations. It extends laterally as shallow as − 7 m over reflector surface SR-3 (Fig. 4), and indicates nearly horizontal and strong continuous internal reflectors in the inner shelf (Figs. 2a and 2c). The lakeward-dipping sedimentary sequence of unit S3 in the seismic profiles (SLD-01 and SLD-05) is represented by moderate to strong continuous reflectors, indicating progradational clinoforms with ca.3 m thickness (Figs. 2b and 3a). On the NW of the lake, the same unit (S3) in seismic profile SLD-11 indicates depositional mounds with ca.11 m thickness, in which undulatory nature of reflection surfaces SR-3 and SR-2 is documented below − 20 m (Fig. 3b). These mounds in the SE of the lake show a conical shape, whereas smoothed and sub-rounded morphology can be documented in the other parts of the lake. According to the HR seismic profiles, the length of these mounds is recorded up to 1.5 km. The most remarkable seismic facies of unit S3 in the seismic profiles is recognized by oblique clinoforms with acoustically strong internal reflectors between the main reflection surfaces SR-3 and SR-2 in the inner shelf, representing prograding foresets of a deltaic-complex (Fig. 4). On the basis of the estimated seismic velocity (~ 1550 m/s), the foreset beds in the deltaic unit are marked by high-amplitude internal reflectors with ~ 3 m thickness, indicating dips of 4–8°. In seismic profile SLD-07, the foresets are truncated at their top by reflection surface SR-2 (Fig. 4). The foreset-topset transition of this deltaic unit occurs at water depth of 19 m.

The overlying unit S2 in the HR seismic profiles indicates strong continuous internal reflectors on the inner shelf with local evidence of coastal onlapping (Figs. 2b and 3a). In seismic profile SLD-01, it extends toward the inner shelf to a water depth of at least 7 m (Fig. 2). This unit (S2) also displays moderate to strong continuous sub-horizontal reflectors with a maximum thickness of 3 m on the deeper side of the lake (Figs. 2c and 3a). In the NW of the lake, unit S2 appears as channel-fills characterized by wedge-shaped lenticular mud drape deposited above the channel-like nature of reflection surface SR-2 (Fig. 3b). In seismic profile SLD-07 from the SW of the lake (Fig. 4), unit S2 is also represented by oblique clinoforms with acoustically strong reflectors, reflecting a deltaic succession in unit S2 between reflection surfaces SR-2 and SR-1 as superimposed on the older one. In the seismic profile, the thickness of this deltaic deposit is around 3.5 m, comparatively thicker than the older one (in unit S3) (Fig. 4). The foreset height ranges between 1 and 1.5 m, and its transition with topset occurs at a water depth of 8.5 m. The foresets are capped by flat-lying reflection surfaces, representing the topset of the deltaic succession. According to the architectural features in the seismic profile (Fig. 4), the deltaic succession of unit S2 comprises lower progradational foresets and upper aggradational topset beds. The basinward equivalence of the deltaic deposits in seismic profile SLD-07 is penetrated by core Salda-2 (Fig. 4), whereas the same unit in seismic profile SLD-01 is also obtained by core Salda2014-P02 on the inner shelf (Fig. 2a).

In the HR seismic profiles, the youngest seismic unit S1 over reflector surface SR-1 is initially represented by moderate to strong continuous horizontal to sub-horizontal internal reflectors in the inner shelf to a water depth of at least 7.5 m (Figs. 2a and 4). The lakeward-dipping sedimentary sequence of unit S1 is confined between the shelf break and slope, indicating weak to moderate continuous reflectors (Figs. 2b and 3a). The thickness of unit S1 reaches 5.5 m in the deeper side of the lake (Fig. 2c), whereas it

displays a thinner succession (< 1.5 m) on the inner shelf (Figs. 2a and 4). This youngest seismic unit is penetrated by cores Salda2014-P02 and Salda-2 (Figs. 2 and 4).

Core lithology

Core Salda2014-P02 was recovered at ~ 29 m water depth from SW of the lake (Fig. 1). The detailed lithostratigraphic analysis of the piston sediment core enables us to differentiate three sedimentary units, labeled as unit L3 to L1, from the base (oldest) to the top (youngest) (Fig. 5). The upper 80 cmblf of core Salda2014-P02 is represented by unit L1, comprising a light gray homogenous clay intercalated with light green laminated silty clay. This youngest unit is associated with highly-fluctuated magnetic susceptibility values (Fig. 6). Unit L2 appears as light olive to olive green silty clays alternated with rosy green clay between 80 and 158 cmblf. This layer is underlain by light gray silty homogenous clay intercalated with olive green clay between 158 and 235 cmblf. Unit L2 as a whole is assigned to a downsection gradual decrease in magnetic susceptibility values (Fig. 6). The upper part of unit L3 between 235 and 278 cmblf in the core is represented by olive to light gray homogenous clays intercalated with rosy green clay. The underlying layer of the same unit until 317 cmblf is composed of dark gray to black homogenous clay with a high organic matter. In the core, a thin veneer of black layer (3020–3050 mm) in unit L3 has been previously determined as a tephra layer based on the physical properties and elemental composition (Ön et al. 2017). The similarity of its geochemical composition with the Minoan eruption provides a high-precision radiocarbon dating at 3560 ± 15 cal years BP (Frederich et al. 2006). A similar tephra layer was previously reported from the other sites of the Anatolian and Aegean regions (Sullivan, 1988; Soles et al. 1995; Eastwood et al. 1998; Aksu et al. 2008; Satow et al. 2015), thus, providing an essential chronostratigraphic marker for the late Holocene time period. The lowermost part of the core below 317 cmblf contains light greenish gray homogeneous clay. The lowermost unit L3 is marked by the least magnetic susceptibility values (Fig. 6).

Core Salda-2 was recovered at ~ 16 m water depth from SW of the lake (Fig. 1). The main lithology in the core is divided into two different lithostratigraphic units, L1 and L2 (Fig. 5). The youngest unit L1 comprises black homogenous clay in the uppermost 8 cmblf. This part of the core is represented by slightly lower magnetic susceptibility values (Fig. 6). An AMS ^{14}C dating obtained from pollen fossils between 57–59 cmblf gives an age of 847+/-25 cal years BP (Fig. 5; Table 2). Downward in the core until 79 cmblf, the rest of unit L1 is represented by a dark gray homogenous clay that is marked by decreasing magnetic susceptibility values (Fig. 6). Unit L2 in the core contains high variable lithologies; the upper part between 79 and 91 cmblf contains yellowish green clay intercalated with dark gray thin clay layers (Fig. 5). The layer down to 98 cmblf comprises alternations of yellowish light and dark green clays. The slight increase in magnetic susceptibility values (Fig. 6) between 108 and 98 cmblf corresponds to a brownish dark green clay layer. This layer is underlain by alterations of dark and light gray clays down to 118 cmblf. The lowermost part of unit L2 between 118 and 129 cmblf is associated with yellowish green and underlying dark gray clay with lower magnetic susceptibility values (Figs. 5 and 6). The other radiocarbon dating in the core obtained from pollen fossils between 132–134 cmblf gives an age of

1870+/-45 cal years BP (Table 2). The lowermost unit L3 at the lowermost 8 cmblf in core Salda-2 is composed of dark greenish gray homogenous clay.

Core-seismic correlation and chronology

In the present study, the determination of the depositional units with an accurate chronology in the studied cores is necessary for precise core-to-seismic correlation and dating the key reflector surfaces of the main sedimentary units in the seismic profiles. The analysis of high-resolution seismic profiles and accurate core logging provides more precise matchings between lithostratigraphic layers recognized in the studied cores (Salda2014-P02 and Salda-2) and seismostratigraphic units in the seismic profiles (SLD-01 and SLD-07) by using synthetic seismograms (Fig. 6). The seismic profiles basically reflect changes in acoustic impedance (i.e., $Z_{ac} = V_p . I_{wbd}$), which do not essentially resemble lithological boundaries or facies changes. However, measured p-wave velocities and density values of a sediment core are the basis for a precise synthetic seismogram that enables precise correlations between seismic and core units. These seismograms were compared with the main seismic reflectors (SR-1, SR-2 and SR-3) in order to confirm the correlation between the sedimentary units and the seismic signal attributed to the facies characterizations of the seismic units. According to the synthetic seismograms, the remarkable reflection surfaces in the seismic profiles coincide with sudden variations in the density and P-wave profiles of the cores (Fig. 6). The main reflection surfaces could be detected in seismograms based on vast amplitude differences rather than other internal reflective layers sandwiched between the main boundaries in the seismic profiles. Amplitudes of the side-oscillations sourced by interbedded sediments were reduced during producing of synthetic seismograms on both cores. Thus, amplitude levels and absorption points of the interbedded sediments are well-detected on down sections, whereas these amplitude peaks are used to detect local boundaries on the age-depth model of core Salda-2 (Figs. 6 and 7).

Chronology of the core sediments with AMS ^{14}C datings is necessary for discussing the timing of different depositional units (L3, L2 and L1) differentiated on the basis of lithological and physical properties of the sediment cores. Adjustment of the radiocarbon-dated chronostratigraphic units in two studied cores correlating with seismic units executed by precisely matching core depths with sub-bottom depths in the HR seismic profiles. Thus, more accurate thickness assignments of the lithostratigraphic units in the cores were established (Fig. 6). The core-to-seismic correlations by using synthetic seismograms indicate that unit L1, L2 and L3 in the cores are the chronostratigraphic equivalence of seismic units from S1 to S3 in the HR seismic profiles. According to the core chronology of the studied cores based on radiocarbon dates (Table 2) and tephrochronology (Minoan tephra), we examine the sedimentary sequence of Lake Salda older than 3560 ± 15 cal years BP (Fig. 7). The age-depth model of core Salda-2 is established by using two radiocarbon ages, and thus, we can tentatively date the lithological boundaries of units L3, L2 and L1 (Fig. 7; Table 2). According to the core chronologies, the youngest unit L1 was deposited during the last 1050 cal year BP, whereas the base of unit L2 was dated at 1690 cal years BP. A single age obtained from the tephra layer (Minoan) in core Salda2014-P02 is not

adequate for a robust age-depth model, which only provides us to estimate an approximate age of unit L3 that must be older than 3560 ± 15 cal years BP. On the basis of correlative stratigraphy in the seismic profiles together with AMS ^{14}C datings in the cores, unit L4 was presumably deposited earlier than the late Holocene.

Lake bathymetry and morphology

The lake expedition with a seismic profiler system carried out in 2019 provided the first bathymetric map of Lake Salda, providing important information about the general morphology of the lake floor (Fig. 8). The bathymetric map shows an overall ellipsoidal-shaped lacustrine basin, having a surface of approximately 43.7 km^2 and a volume of 79.2 km^3. The deepest part of the lake depression close to the SE corner of the lake possesses ~ 192 m water depth, which can be described as a flat basin, forming a slightly upward-concave bowl. Laterally, this deepest part of the lake is surrounded by steep sides, representing the slopes of the lake margin (Fig. 8). The northern and eastern shelves are much wider than the western and southern shelves, surrounded by mostly smooth coastlines. Steep slopes of the lake with angles up to 10° to 12° down to a water depth of ~ 70 to ~ 90 m. Based on the bathymetric and seismic data, the shelf break along both northern and southern shelves occurs at a water depth of 25 m. The SE and NE shores of Lake Salda are bounded by steep slopes due to surrounding mountains that are associated with dense drainage networks. The most extensive drainage systems are Değirmen and Kocakayak rivers, forming the largest present-day delta plains around the lake shoreline (Fig. 8). Several streams and ephemeral creeks draining from the surrounding catchments likely provide a high amount of water and sediments to the lake.

Onshore study

Along the present coastal plain around Lake Salda, a series of ancient lake terraces exist at different elevations, implying past water level variations during the late Holocene (Balcı et al. 2020). The highest lake terrace is documented at ~ 22 m above the present lake level at the eastern part of the lake (site L-2 in Fig. 1b). The terrace deposit at this location consists of beige color clayey hydromagnesite sand with well-rounded pebbles due to well reworking that is likely typical for a deposition at the coastline (Fig. 9). The similar terrace deposits were previously examined at 3 m and 6 m above the present lake level, giving ages of 625 cal years BP and 750 cal years BP (Balcı et al. 2020). Apart from the lake terraces, two prominent deltaic successions are well exposed in road cuts around Lake Salda (sites L-3 and L-1 in Fig. 1b). The eastern deltaic-complex close to Yeşiloava town (site L-1 in Figs. 1b and 10) occupies ~ 10 m above the present lake level (1180 m), whereas the western one at the Salda Village is located at a much higher elevation (1194 m) (site L-3 in Figs. 1b and 10). A thin layer of peat deposit from the eastern deltaic-complex (Fig. 11b) is dated by AMS ^{14}C analysis, giving an age younger than 650 cal years BP (Table 2). Therefore, the delta generation along the coastline timely coincides with deposition of the youngest seismic unit S1 (after 1050 cal years BP) in the lake. According to the sedimentological and

architectural properties, the vertically stacked succession of multiple coarse-grained fan deltas on both sides of the lake are of quite similar origin. Each successive sequence is divisible into bottomset, foreset and topset facies (Figs. 10a and 10d). The bottomset facies in the lower sequence of both deltaic complexes comprises alternations of low-lying thin layers of fine sandy clays and pebbly fine sand. The foresets of each deltaic sequence separate subhorizontal topset and bottomset beds, and indicate steep (~ 11–16˚) clinoform beds with thicknesses ranging from 15 to 0.45 m (Figs. 10a and 10d). It consists of poorly to moderately sorted conglomerate intercalated with better-sorted medium to coarse-grained conglomeratic sandstones (Fig. 10e). However, foresets are truncated by topsets in the deltaic sequences that are made up of relatively thinner beds of poorly-sorted pebbly sandstones alternated with muddy sandstones and sandy mudstones with a high amount of organic material (Figs. 10b and 10c). The pebbles in the topset, foreset and bottomset beds are sub-angular to sub-rounded, and derived mostly from ultramafic rocks and limestone.

Discussion

Depositional settings of sedimentary units

The source and period of the sedimentary sequence in the lake can be confidently deduced from the correlation of ^{14}C-dated onshore outcrops and depositional units described in the high-resolution (HR) seismic reflections profiles with the chronostratigraphic units in the cores. The internal seismic configurations of the sedimentary successions in the HR seismic profiles (units S4 to S1) reveal different depositional conditions in the lake, each subject to distinctive hydrological and sedimentological processes, implying a dynamic depositional history with respect to changing water level and climate conditions. The oldest sedimentary unit S4 over the acoustic basement in the HR seismic profiles could not be penetrated by the sediment core, but its age can be confidently deduced from the correlation of the seismic stratigraphic units with the chronostratigraphic units in the cores. According to the core chronologies together with the synthetic seismograms (Figs. 6 and 7), the age of unit S3 is estimated to be much older than 3560 ± 15 cal years BP (Fig. 11), thus, the older unit S4 might have possibly been deposited in the lake during the earlier phase of middle Holocene (~ 4.200 cal years BP). The internal seismic configurations such as conformable parallel beds with lakeward thickening (Fig. 2c) and slightly inclined clinoforms (Figs. 2b and 3a) are evidence for a regressive deposition in Lake Salda.

In the HR seismic profiles, the various seismic internal configurations of the younger unit S3 between SR-3 and SR-2 reflection surfaces indicate distinct depositional facies deposited in the lake until 1690 cal year BP during the late Holocene. The most remarkable facies of this unit is recorded as an acoustically chaotic internal configuration in seismic profile SLD-11 (Fig. 3b), indicating the formation of a stromatolite in the lake. Its present form was previously described as hydrated Mg-carbonates stromatolites along the present shoreline of the lake (Balcı et al. 2020). On the other hand, the lakeward-dipping seismic configuration of unit S3 deposited as thick clinoforms between SR-3 and SR-2 reflector surfaces (Figs. 2b and 3a) provides strong evidence for progradational shoreface facies. The

stratigraphic equivalence of the same unit in seismic profile SLD-07 consists of oblique clinoforms, implying the existence of a buried delta-complex (Fig. 4). The general clinoform architecture of this deltaic sediment is represented by the foreset bed with dips ranging between 4° and 8°. Therefore, the depositional mode could have been river-dominated, implying hyperpycnal mixing in the lake during the delta deposition. The termination of delta progradation in the lake timely coincides with the formation of remarkable erosion along the reflector surface SR-2 (Fig. 4) that has removed topsets from the lakeward rim of the deposit. Contrariwise, the channel-like nature of the same reflection surface (SR-2) in seismic profile SLD-11 (Fig. 3b) is considered to have resulted from the submerged channel incision soon after deposition of the mounded stromatolite (1690 cal years BP) due to the progradation of fluvial systems along the lake catchment.

The migration of the deltaic system further inland produced a younger deltaic-complex in unit S2 between seismic reflectors SR-2 and SR-1 in seismic profile SLD-07 (Fig. 4). According to seismic-to-core correlation together with the age-depth model of core Salda-2 (Figs. 6 and 7), the superimposed deposition of this younger deltaic unit (S2) over the older one in unit S3 took place in the lake between 1690 and 1050 cal years BP. However, the transgressive nature of unit S2 is also evidenced by channel-fills (Fig. 3b) and coastal onlapping seismic configurations (Figs. 2b and 3a). The youngest depositional seismic unit S1 could have been deposited during the last 1050 cal years BP as parallel-bedded mud drape, covering the older sedimentary units in the HR seismic profiles (Figs. 2–4).

In addition to the seismic stratigraphic units in HR seismic profiles, the latest Holocene sedimentary onshore sequence along the coastal plain of the lake is represented by the deposition of Gilbert-type fan delta, attesting to the possible interaction between tectonic and the depositional condition in the lake. According to the radiocarbon date from a peat layer in the delta topset (Fig. 10b; Table 2), the accelerated tectonism along the lake margin around 650 cal years BP episodically provided an environment suitable for fan-delta formation by creating marked topographic relief and accommodation space in the lake. The lack of well-developed stratification and cross-bedding may be due to rapid deposition with little or no reworking. However, the absence of wave and storm-stratification features within the foreset and topset beds point to a gravelly fan deltaic system in which the receiving basin may have been a low-energy, protected lake embayment.

Implications for lake level and climate changes

The seismic-to-core matchings by using the synthetic seismograms (Fig. 6) allow us to calibrate seismic stratigraphic units and serve to explore the chronology of the lake level changes due to paleoclimate variations. Each of these units represents various depositional facies that could be attributed to the high variations in lake level, likely controlled by the local climate and sediment availability. The multi-proxy records from the Eastern Mediterranean lakes indicate a series of downward trending wet-to-dry oscillations during the mid-to-late Holocene (Roberts et al. 2011). During this period, remarkable climate oscillations and water level changes took place in the Anatolian lakes, as indicated by the proxy-climate

data (Kempe et al. 2002; Wick et al. 2003; Jones et al. 2006; Litt et al. 2009; Kuzucuoğlu et al. 2011; Eriş, 2013; Çağatay et al. 2014; Eriş et al. 2018). Although the seismic configuration of unit S4 could not be recorded continuously in the HR seismic profiles, its general seismic configuration (Figs. 2b, 2c and 3a) suggests regressive deposition due to lake level decrease due to the prevailing dry climate during the late phase of middle Holocene (prior ~ 4,200 cal years BP). However, general aridification during the mid-Holocene was also inferred from $d^{18}O$ and $d^{13}C$ records of speleothems in Israel (Bar- Matthews et al. 2000), and by geochemistry and pollen data from crater-lake sediments in central Turkey (Roberts et al. 2001).Since the deposition of unit S4 could not take place above the minimum depth of the overlying reflector surface SR-3 in the HR seismic profiles (Figs. 2–4), the possible water depth during its deposition in the lake could not have exceeded − 10 m.

The distinct seismic reflection configurations of unit S3 reveal different depositional facies that is likely attributed to variations in the depositional conditions across the lake. The lake level decrease during its deposition is inferred from the lakeward-dipping clinoforms recorded in seismic profile SLD-01 (Fig. 2a). The most prominent evidence for progradational facies of the same seismic unit (S3) is also evidenced by the existence of river-dominated deltaic deposition in seismic profile SLD-07 (Fig. 4). The possible reason for a progradational deposition in the lake could be explained by subsequent lake level decrease due to continuous dry climate until 1690 cal years BP. The same arid interval around Lake Salda correlates with similar hydrological conditions in Lake Van, Lake Tecer, Lake Nar and Lake Hazar (Lemcke and Sturm, 1997; Kempe et al. 2002; Landmann and Kempe, 2005; Eriş et al. 2018). The relatively finer grain composition together with lower magnetic susceptibility value (Figs. 5 and 6) of unit L3 in core Salda2014-P02 indicate low detrital input to the lake due to drier climate conditions (Fig. 11). Moreover, the sediment supply during the deltaic deposition could have exceeded the available accommodation space as a result of the enhanced water level decrease in the lake, which was quickly filled with sediment, leading to a coastal regression. In the seismic profile (Fig. 4), the topset/foreset transition of the deltaic deposit of unit S3 occurs at − 15 m, implying a minimum lake level during the entire period of growth of this deltaic sequence in the lake. A similar delta progradation under a general dry climate condition was previously recorded from Lake Hazar in eastern Anatolia on the basis of seismic and core data (Eriş 2013; Eriş et al. 2018). The another unique facies association of unit S3 in the lake is documented as an extensive and thick (~ 11 m) stromatolite formation (Fig. 3b) that could be likely promoted by oligotrophic conditions due to a dry climate. According to the age interval of unit L3 in the cores (older than 1650 cal years BP), the formation of extensive stromatolite in the lake timely coincides with the Roman Warm Period (2600 and 1550 cal years BP, Wick et al. 2003; Tudryn et al. 2013). Such phenomenon indicates that the mid-Holocene humid phase associated with African monsoon forcing apparently was also more weakened around Lake Salda at the beginning of the late Holocene. According to other paleo-proxy records from well-dated sediment cores in the Anatolian lakes (Lemcke and Sturm 1997; Kempe et al. 2002; Landmann and Kempe 2005; Kuzucuoglu et al. 2011; Roberts et al. 2011; Ülgen et al. 2012), the cold and dry climatic condition during the same period gave rise to significant lake level drops. The late Holocene in Anatolia is represented by water level decreases in lakes due to cold and dry climatic conditions initiated at around 3.0 ka BP (Eriş et al. 2018). The arid climate during the same

period prevailed in the northeastern Mediterranean, as indicated by isotope data (Roberts et al. 2008, 2011b; Leng et al. 2013) and lake-level reconstructions (Harrison and Digerfeldt, 1993; Digerfeldt et al. 2007; Magny et al. 2011). However, the positive excursion in the $\delta^{13}C$ record at Sofular Cave in the same interval indicates diminished precipitation (Fleitmann et al. 2009).

The termination of the delta formation of unit S3 in the seismic profile (Fig. 4) during the late Holocene was accompanied by erosion along reflector surface SR-2 that partly removed topsets prior to the subsequent phase of the younger deltaic deposit in unit S2. In addition, the progradation of the fluvial system at the catchment area during the same time can be inferred from the undulatory surface characteristic and channel-incision over the same reflector surface (SR-2) in seismic profile SLD-11 (Fig. 3b). On the basis of seismic-to-core correlation (Figs. 4 and 6), this prominent erosional truncation corresponds to the sharp lithologic boundary between units L3 and L2 in core Salda-2 (Fig. 5), suggesting an abrupt facies change in the lake as a result of further water level decrease. According to the core chronology (Figs. 5 and 7), the timing of this regressive phase of the lake must be younger than 1690 cal years BP. Such remarkable climate deterioration due to a continuous dry climate during the termination of Roman Warm Period has been previously documented in the Nar and Tecer lakes (Jones et al. 2006; Kuzucuoğlu et al. 2011).

After a brief water-level decrease in Lake Salda prior to the deposition of unit S2 (~ 1690 cal years BP), initiation of transgressive lake level produced a younger deltaic complex of unit S2 as superimposed on the older deltaic deposit in unit S3 (Fig. 4), implying the migration of the coastal deposition further inland. This new deltaic unit (S2) is different with having a lesser inclination of the foresets and a prominent aggradational topset. Such seismic configuration likely suggests that deltaic deposition took place when sediment supply rate never caught up the lake level rise due to continuously increased precipitation soon after 1690 cal years BP. Nevertheless, this circumstance would have induced a relatively highest sedimentation rate (2.1 mm/year) during the unit S2 deposition (Fig. 11) based on the age-depth model of core Salda-2 (Fig. 7), although it progressively decreased towards the termination of this unit. The lithostratigraphic equivalence of this seismic unit (S2) in the studied cores (unit L2) is represented by the coarser-grained lithology together with elevated magnetic susceptibility values (Figs. 5 and 6), implying higher detrital input to the lake due to a wetter climate. The water depth of the topset/foreset transition (– 8.5 m) in the younger deltaic sequence in seismic profile SLD-07 (Fig. 4) is 6.5 m shallower than the older one as a result of lake level rise. This younger deltaic deposition (1690 – 1050 cal years BP) under a wetter climate condition timely coincides with the onset of the Dark Age period, initiating after 1600 cal years BP in the late Holocene. In the HR seismic profiles, other implications for a transgressive lake level during the unit S2 deposition are documented by other seismic configurations such as coastal onlapping (Fig. 3a) and wedge-shaped lenticular channel-fills (Fig. 3b).

According to the onshore observations around Lake Salda (sites L-1 and L-3 in Fig. 1b), the formation of thick sequences of Gilbert-type fan deltas (Fig. 10) during the last 650 cal years BP suggests a possible interaction between tectonic and the lake level in the latest Holocene. Their deposition could be attributed to a brief period of extremely rapid basin subsidence, resulting in a deepening of the lake. Comparison of

elevations of the delta outcrops (1190–1194 m) with the present lake level (1180 m) implies that the higher lake level in compare to earlier period of the late Holocene (prior to ~ 650 cal years BP) must have been existed during the deltaic deposition. Considering the chronology seismic units, the formation of Gilbert-type fan deltas along the coastline is almost timely equivalence of seismic unit S1 (younger than 1050 cal years BP) deposited in the lake. Its lithostratigraphic equivalence in core Salda-2 is represented by dark to black homogenous clay due to high organic matter content (Fig. 5), likely implying a warm and productive lake during the same period. The seismic configuration of this unit (Figs. 2–4) in the HR seismic profiles reveals a transgressive mud drape deposited over the older seismic units (S3 and S2) during the increased lake level. Another evidence of a higher lake level during the latest Holocene is documented by the existence of an ancient lake terrace at ~ 22 m above the present lake level (Fig. 9). The ages of similar ancient lake terraces along the present coastline gives 625 cal years BP and 750 cal years BP (Balcı et al. 2020), timely coinciding with the fan delta deposition during higher water level in the lake in the latest Holocene.

Conclusion

Seismic–stratigraphic and chronostratigraphic analyses of the sedimentary sequence in Lake Salda provide important information on sedimentation and lake level changes during the mid-to-late Holocene. This study mainly contains offshore and onshore studies, including lithology of sediment cores, high-resolution seismic profiles and sediment outcrops along the present coastline. Integrating the high-resolution seismic and sediment core data provide correlating seismic stratigraphic units and core lithologies, which allowed us to establish an accurate chronology of the sedimentary successions deposited in the lake. Based on the detailed core lithology together with seismic reflection configurations, different depositional units are distinguished within the sedimentary sequence of Lake Salda, covering the time period beyond 3560 cal year BP. At the core sites, the overall succession of sediments observed in the high-resolution seismic profile consists of four depositional units, i.e., S4 to S1 from the bottom to top, reflecting high variations in the past water level in Lake Salda. The termination of the middle Holocene is marked by progradational shoreface facies of unit S4 in the seismic profiles, likely reflecting the low lake level due to the dry climate. The later depositional period until 1690 cal year BP is accompanied by the further lake level decrease that produced the lakeward-dipping seismic configuration of the overlying unit S3 on the lake slopes and delta progradation in the inner shelf of the lake. This regressive depositional period coincided with the formation of stromatolite along the lake floor during the Roman Warm Period. The return to a wetter climate period after 1690 cal year BP is documented by the retreat of the river-dominated deltaic deposition further inland, implying transgressive lake level until 1050 cal year BP. The formation of Gilbert-type fan delta along the present coastline of the lake implies a higher lake level during the last 650 cal year BP, which is also evidenced by ancient lake terraces above the present lake level.

Declarations

Author contributions

Asen Sabuncu: Data curation, Methodology, Resources, Software, Visualization, Writing - Original Draft. Kürşad Kadir Eriş: Project administration, Funding acquisition, Supervision, Formal analysis, Writing-review & editing. Gülsen Uçarkuş: Conceptualization, Methodology. Dursun Acar: Data Curation, Resources. Erdem Kırkan: Data Curation, Resources, Visualization. Nurettin Yakupoğlu: Data Curation, Resources, Software. Sena Akçer Ön: Project administration, Funding acquisition, Supervision, Resources. Nurgul Balci: Investigation, Validation, Resources.

Data availability

All experimental Data derivated from sediment cores will be made available on ITU-EMCOL repository: http://www.emcol.itu.edu.tr/Icerik.aspx?sid=12388

Declaration of competing interest

The authors declare that they have no known competing financial interests or personal relationships that could have appeared to influence the work reported in this paper.

Acknowledgments

This study was part of Asen Sabuncu' PhD Thesis and supported by Higher Education Council of Turkey (YOK, 100/2000 PhD Scholarship). We would like to thank all fieldwork members who attended two coring campaigns during 2014 and 2017 in Lake Salda. We are also thankful to Ayşe Kaşlılar (Uppsala University) and Emin Demirbağ (İstanbul Technical University) for assisting to developed seismogram scripts, IHS for their academic donations, and undergraduate students for their help during the core analyses.

Funding

This study has been supported by the Scientific and Technological Research Council of Turkey (TÜBİTAK, Project number: 113Y408), Istanbul Technical University Research Fund (ITU-BAP, Project number: 41244).

References

1. Aksu AE, Jenner G, Hiscott RN, İşler EB (2008) Occurrence stratigraphy and geochemistry of Late Quaternary tephra layers in the Aegean Sea and the Marmara Sea. Mar. Geol 252(3-4): 174-192
2. Balcı N, Demirel C, Ön SA, Gültekin AH, Kurt MA (2018) Evaluating abiotic and microbial factors on carbonate precipitation in Lake Acigöl a hypersaline lake in Southwestern Turkey. Quat. Int 486:116-128
3. Balcı N, Günes Y, Kaiser J, Ön SA, Eriş KK, Garczynski B, Horgan BH (2020) Biotic and Abiotic Imprints on Mg-Rich Stromatolites: Lessons from Lake Salda SW Turkey. Geomicrobiol. J 37(5):401-425

4. Bar-Matthews M, Ayalon A, Kaufman A.: (2000) Timing and hydrological conditions of Sapropel events in the Eastern Mediterranean as evident from speleothems Soreq cave Israel. Chem. Geol 169(1-2):145-156
5. Blaauw M (2010) Methods and code for ‘classical’age-modelling of radiocarbon sequences. Quat. Geochron 5(5):512-518
6. Boës X, Moran SB, King J, Cağatay MN, Ferrari AH (2010) Records of large earthquakes in lake sediments along the North Anatolian Fault Turkey. J. Paleolimnol 43(4):901-920
7. Braithwaite CJR, Zedef V (1994) Living hydromagnesite stromatolites from Turkey. Sediment. Geol 92(1-2):1-5
8. Braithwaite CJR, Zedef V (1996) Hydromagnesite stromatolites and sediments in an alkaline lake Salda Golu Turkey. J. Sediment. Res 66(5):991-1002
9. Çağatay MN, Öğretmen N, Damcı E, Stockhecke M, Sancar Ü, Eriş KK, Özeren S (2014) Lake level and climate records of the last 90 ka from the Northern Basin of Lake Van eastern Turkey. Quaternary Sci. Rev 104:97-116
10. Çaldırak H, Kurtuluş B, Canoğlu MC, Tunca E (2017) Assessment of heavy metal contamination and accumulation patterns in the coastal and deep sediments of Lake Salda Turkey. Fresen Environ Bull 8047
11. Danladi IB, Ön SA, (2018) Solar forcing and climate variability during the past millennium as recorded in a high altitude lake: Lake Salda (SW Anatolia). Quat. Int 486:185-198
12. Davraz A, Varol S, Sener E, Aksever F, Kırkan B, Tokgözlü A (2019) Assessment of water quality and hydrogeochemical processes of Salda alkaline lake (Burdur Turkey). Environ. Monit. Assess 191(11):1-18
13. Dereli MA, Tercan E (2020) Assessment of shoreline changes using historical satellite images and geospatial analysis along the Lake Salda in Turkey. Earth Sci. Inform 13(3):709-718
14. Digerfeldt G, Sandgren P, Olsson S (2007) Reconstruction of Holocene lake-level changes in Lake Xinias central Greece. Holocene 17(3):361-367
15. Eastwood WJ, Pearce NJ, Westgate JA, Perkins WT (1998) Recognition of Santorini (Minoan) tephra in lake sediments from Gölhisar Gölü southwest Turkey by laser ablation ICP-MS. J. Archaeol. Sci 25(7):677-687
16. Eriş KK (2013) Late Pleistocene–Holocene sedimentary records of climate and lake-level changes in Lake Hazar eastern Anatolia Turkey. Quat. Int 302:123-134
17. Eriş KK, Ön SA, Çağatay MN, Ülgen UB, Ön ZB, Gürocak Z, Okan ÖÖ (2018) Late Pleistocene to Holocene paleoenvironmental evolution of Lake Hazar Eastern Anatolia Turkey. Quat. Int 486:4-16
18. Fleitmann D, Cheng H, Badertscher S, Edwards RL, Mudelsee M, Göktürk OM, Tüysüz O (2009) Timing and climatic impact of Greenland interstadials recorded in stalagmites from northern Turkey. Geophys. Res. Lett 36(19)

19. Friedrich WL ,Heinemeier J (2009) The Minoan eruption of Santorini radiocarbon dated to 1613+ 13 BC-geological and stratigraphic considerations. Monographs of the Danish Institute at Athens (MoDIA) 10:57-63
20. Harrison SP, Digerfeldt G (1993) European lakes as palaeohydrological and palaeoclimatic indicators. Quaternary Sci. Rev 12(4):233-248
21. Horgan BH, Anderson RB, Dromart G, Amador ES, Rice MS (2020) The mineral diversity of Jezero crater: Evidence for possible lacustrine carbonates on Mars. Icarus 339:113526
22. Jones MD, Roberts CN, Leng MJ, Türkeş M (2006) A high-resolution late Holocene lake 674 isotope record from Turkey and links to North Atlantic and monsoon climate. Geology 34(5) 675:361-364
23. Kaiser J, Ön ZB, Arz HW, Ön SA (2016) Sedimentary lipid biomarkers in the magnesium-rich and highly alkaline Lake Salda (south-western Anatolia). J. Limnol 75(3)
24. Kazancı N, Girgin S, Dügel M (2004) On the limnology of Salda Lake a large and deep soda lake in southwestern Turkey: future management proposals. Aquat. Conserv 14(2):151-162
25. Kazancı N, Girgin S, Dügel M, Oğuzkurt D, Mutlu B, Dere Ş, Özçelik M (1999) Researches on inland waters of Turkey IV: Limnology Environmental Quality and Biological Diversity of Koycegiz, Beysehir, Egirdir, Aksehir, Eber, Çorak, Kovada, Yarıslı, Bafa, Salda, Karatas, Cavuscu Lakes, Buyuk and Kucuk Menderes Deltası, Gulluk vand Karamuk Marshy Areas. Imaj Press: Ankara
26. Kempe S, Landmann G, Müller G (2002) A floating varve chronology from the last glacial maximum terrace of lake Van (Turkey). Z. Geomorphol Supp126:97-114
27. Kocaefe S, Ataman G (1976) Actual tectonics of the Western Anatolia. Yerbilimleri 9:149-162
28. Kotthoff U, Pross J, Müller UC, Peyron O, Schmiedl G, Schulz H, Bordon A (2008) Climate dynamics in the borderlands of the Aegean Sea during formation of sapropel S1 deduced from a marine pollen record. Quaternary Sci. Rev 27(7-8):832-845
29. Kuzucuoğlu C (2007) Climatic and environmental trends during the third millennium BC in Upper Mesopotamia. Publications de l'Institut Français d'Études Anatoliennes 19(1):459-480
30. Kuzucuoğlu C, Dörflez W, Kunesch S, Goupille F (2011) Mid-to late-Holocene climate change in central Turkey: The Tecer Lake record. The Holocene 21(1):173-188
31. Landmann G, Kempe S (2005) Annual deposition signal versus lake dynamics: microprobe analysis of Lake Van (Turkey) sediments reveals missing varves in the period 11.2–10.2 ka BP. Facies 51(1-4):135-145
32. Lemcke G, Sturm M (1997) δ18O and trace element measurements as proxy for the reconstruction of climate changes at Lake Van (Turkey): Preliminary results. In Third millennium BC climate change and Old World collapse. Springer, Berlin
33. Leng MJ, Wagner B, Boehm A, Panagiotopoulos K, Vane CH, Snelling A, Baneschi I (2013) Understanding past climatic and hydrological variability in the Mediterranean from Lake Prespa sediment isotope and geochemical record over the Last Glacial cycle. Quaternary Sci. Rev 66:123-136

34. Leroy S, Kazancı N, İleri Ö, Kibar M, Emre O, McGee E, Griffiths HI (2002) Abrupt environmental changes within a late Holocene lacustrine sequence south of the Marmara Sea (Lake Manyas NW Turkey): possible links with seismic events. Mar. Geol 190(1-2):531-552
35. Leroy S, Boyraz S, Gürbüz A (2009) High-resolution palynological analysis in Lake Sapanca as a tool to detect recent earthquakes on the North Anatolian Fault. Quaternary Sci. Rev 28(25-26):2616-2632
36. Leroy S, Schwab MJ, Costa PJ (2010) Seismic influence on the last 1500-year infill history of Lake Sapanca (North Anatolian Fault NW Turkey). Tectonophysics 486(1-4):15-27
37. Litt T, Pickarski N, Heumann G, Stockhecke M, Tzedakis PC (2014) A 600000 year long continental pollen record from Lake Van eastern Anatolia (Turkey). Quaternary Sci. Rev 104:30-41
38. Magny M, Vannière B, Calo C, Millet L, Leroux A, Peyron O, Tinner W (2011) Holocene hydrological changes in south-western Mediterranean as recorded by lake-level fluctuations at Lago Preola a coastal lake in southern Sicily Italy. Quaternary Sci. Rev 30(19-20) :2459-2475
39. Mavromatis V, Bundeleva IA, Shirokova LS, Millo C, Pokrovsky OS, Benezeth P, Oelkers EH, (2015) The continuous re-equilibration of carbon isotope compositions of hydrous Mg carbonates in the presence of cyanobacteria. Chem. Geol 404:41-51
40. Ocakoğlu F, Çilingiroğlu Ç, Erkara İP, Ünan S, Dinçer B, Akkiraz MS (2019) Human-climate interactions since the neolithic period in Central Anatolia: Novel multi-proxy data from the Kureyşler area Kütahya Turkey. Quaternary Sci. Rev 213:1-17
41. Ön SA, Sakınç M, Eriş KK, Akkiraz S, Gündoğan İ, Büyükmeriç Y, Sancar Ü, Ön ZB, Acar D (2018) Quaternary period paleoclimate of Southwest Anatolia and its surroundings: climate records in Acıgöl (Denizli-Afyonkarahisar) and Salda Lake (Burdur) and their comparison with global records. Environment Atmospheric Earth and Marine Sciences Research Support Group Technical Report No. 113Y408. The Scientific and Technological Research Council of Turkey
42. Reimer PJ, Austin WE, Bard E, Bayliss A, Blackwell PG, Ramsey CB, Talamo S (2020) The IntCal20 Northern Hemisphere radiocarbon age calibration curve (0–55 cal kBP). Radiocarbon 62(4):725-757
43. Roberts N, Jones MD, Benkaddour A, Eastwood WJ, Filippi ML, Frogley MR, Zanchetta G (2008) Stable isotope records of Late Quaternary climate and hydrology from Mediterranean lakes: the ISOMED synthesis. Quaternary Sci. Rev 27(25-26):2426-2441
44. Roberts N, Moreno A, Valero-Garcés BL, Corella JP, Jones M, Allcock S, Türkeş M (2012) Palaeolimnological evidence for an east–west climate see-saw in the Mediterranean since AD 900. Global. Planet. Change 84:23-34
45. Roberts N, Reed JM, Leng MJ, Kuzucuoğlu C, Fontugne M, Bertaux J, Karabiyikoğlu M (2001) The tempo of Holocene climatic change in the eastern Mediterranean region: new high-resolution crater-lake sediment data from central Turkey. The Holocene 11(6) 721-736 (2001).
46. Russell MJ, Ingham JK, Zedef V, Maktav D, Sunar F, Hall AJ, Fallick AE (1999) Search for signs of ancient life on Mars: expectations from hydromagnesite microbialites Salda Lake Turkey. J. Geol. Soc. London 156(5):869-888

47. Salvatore M.R, Goudge T.A, Bramble M.S, Edwards C.S, Bandfield JL, Amador ES Christensen PR (2018) Bulk mineralogy of the NE Syrtis and Jezero crater regions of Mars derived through thermal infrared spectral analyses. Icarus 301:76-96
48. Sarp H (1976) Etude geoloqique et petropraphique du Cortege Ophiolitique de la Region Situee au Nord-Ouest de Yeşilova (Burdur-Turkey). Thesis University of Geneve
49. Satow C, Tomlinson EL, Grant KM, Albert PG, Smith VC, Manning CJ, Menzies MA (2015) A new contribution to the Late Quaternary tephrostratigraphy of the Mediterranean: Aegean Sea core LC21. Quaternary Sci. Rev 117:96-112
50. Schmid H (1987) Turkey's Salda Lake. A genetic model for Australia's newly discovered magnesite deposits. IND. MINER. Ind. Miner 239:19
51. Schmiedl G, Kuhnt T, Ehrmann W, Emeis KC, Hamann Y, Kotthoff U, Pross J. (2010) Climatic forcing of eastern Mediterranean deep-water formation and benthic ecosystems during the past 22 000 years. Quaternary Sci. Rev 2923-24:3006-3020
52. Schwab MJ, Werner P, Dulski P, McGee E, Nowaczyk NR, Bertrand S, Leroy S (2009) Palaeolimnology of Lake Sapanca and identification of historic earthquake signals northern Anatolian fault zone (Turkey). Quaternary Sci. Rev 28(11-12):991-1005
53. Shirokova LS, Mavromatis V, Bundeleva I, Pokrovsky OS, Bénézeth P, Pearce C, Oelkers EH (2011) Can Mg isotopes be used to trace cyanobacteria-mediated magnesium carbonate precipitation in alkaline lakes?. Biogeosci.Disc 8(4):6473-6517
54. Shirokova LS, Mavromatis V, Bundeleva IA, Pokrovsky OS, Bénézeth P, Gérard E, Oelkers EH (2013) Using Mg isotopes to trace cyanobacterially mediated magnesium carbonate precipitation in alkaline lakes. Aquat. Geochem 19(1):1-24
55. Soles JS, Taylor SR, Vitaliano CJ (1995) Tephra samples from Mochlos and their chronological implication for Neopalatial Crete. Archaeometry 37(2):385-393
56. Sullivan DG (1988) The discovery of Santorini Minoan tephra in western Turkey. Nature 333(6173):552-554
57. Şenel M, Selçuk H, Bilgin ZR, Şen AM, Karaman T, Dinçer MA, Durukan E, Arbas A, Örçen S, Bilgi C (1989) Geology of Çameli (Denizli) - Yeşilova (Burdur) and north part of the Elmalı (Antalya) regions. General Directorate of Mineral Research and Exploration Report No: 9429 Ankara
58. Tudryn A, Tucholka P, Özgür N, Gibert E, Elitok O, Kamaci Z, Platevoet B (2013) A 2300-year record of environmental change from SW Anatolia Lake Burdur Turkey. J. Paleolimnol 49(4):647-662
59. Tzedakis PC (2007). Seven ambiguities in the Mediterranean palaeoenvironmental narrative. Quaternary Sci. Rev 26(17-18):2042-2066
60. Ülgen UB, Franz SO, Biltekin D, Çagatay MN, Roeser PA, Doner L, Thein J (2012) Climatic and environmental evolution of Lake Iznik (NW Turkey) over the last~ 4700 years. Quat. Int 274 :88-101
61. Weaver PPE, Schultheiss PJ (1990) Current methods for obtaining logging and splitting marine sediment cores. Mar. Geophys. Res 12(1-2):85-100

62. White RE (1980) Partial coherence matching of synthetic seismograms with seismic traces. Geophys. Prospect 28(3):333-358
63. Wick L, Lemcke G, Sturm M (2003) Evidence of Lateglacial and Holocene climatic change and human impact in eastern Anatolia: high-resolution pollen charcoal isotopic and geochemical records from the laminated sediments of Lake Van Turkey. The Holocene 13(5): 665-675
64. Zedef V, Russell MJ, Fallick AE, Hall AJ (2000) Genesis of vein stockwork and sedimentary magnesite and hydromagnesite deposits in the ultramafic terranes of southwestern Turkey: a stable isotope study. Econ. Geol. 95(2):429-445

Figures

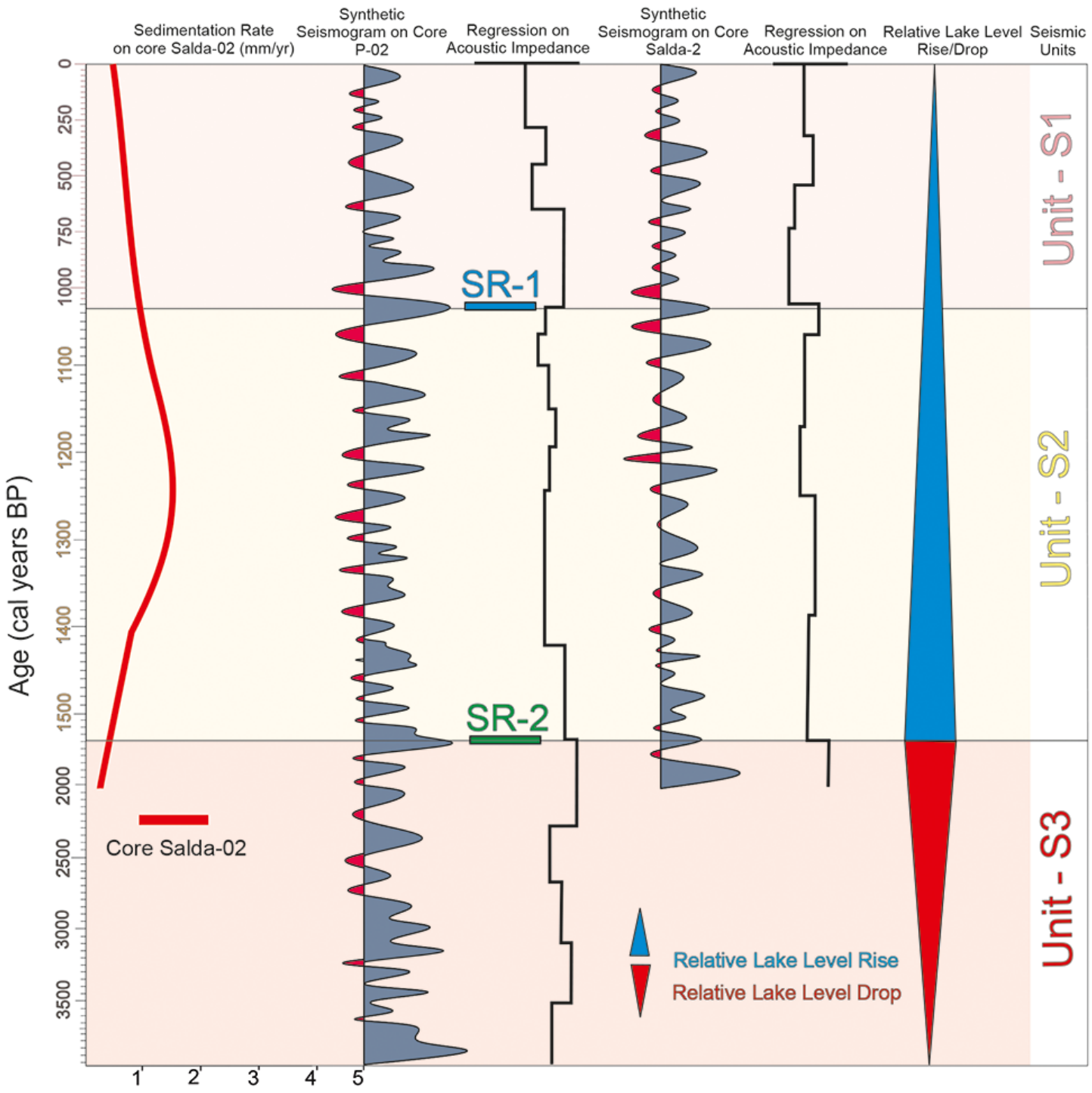

Figure 1

a) Simplified map showing the location of Lake Salda in the northwest of Turkey. **b)** A DEM map (digital elevation model) based on Satellite Radar Topography Mission (SRTM) indicating the present topography of the catchment area around Lake Salda. The map also shows locations of the studied sediment cores (green dots) and onshore outcrops (red dots) and high-resolution seismic reflection profiles (dashed dark blue lines) collected during lake surveys of 2014 and 2017. The locations of L-1 and L-3 (red dots) along the present coastline represent the delta outcrops, and L-2 indicates the location of the highest lake terrace documented in this study.

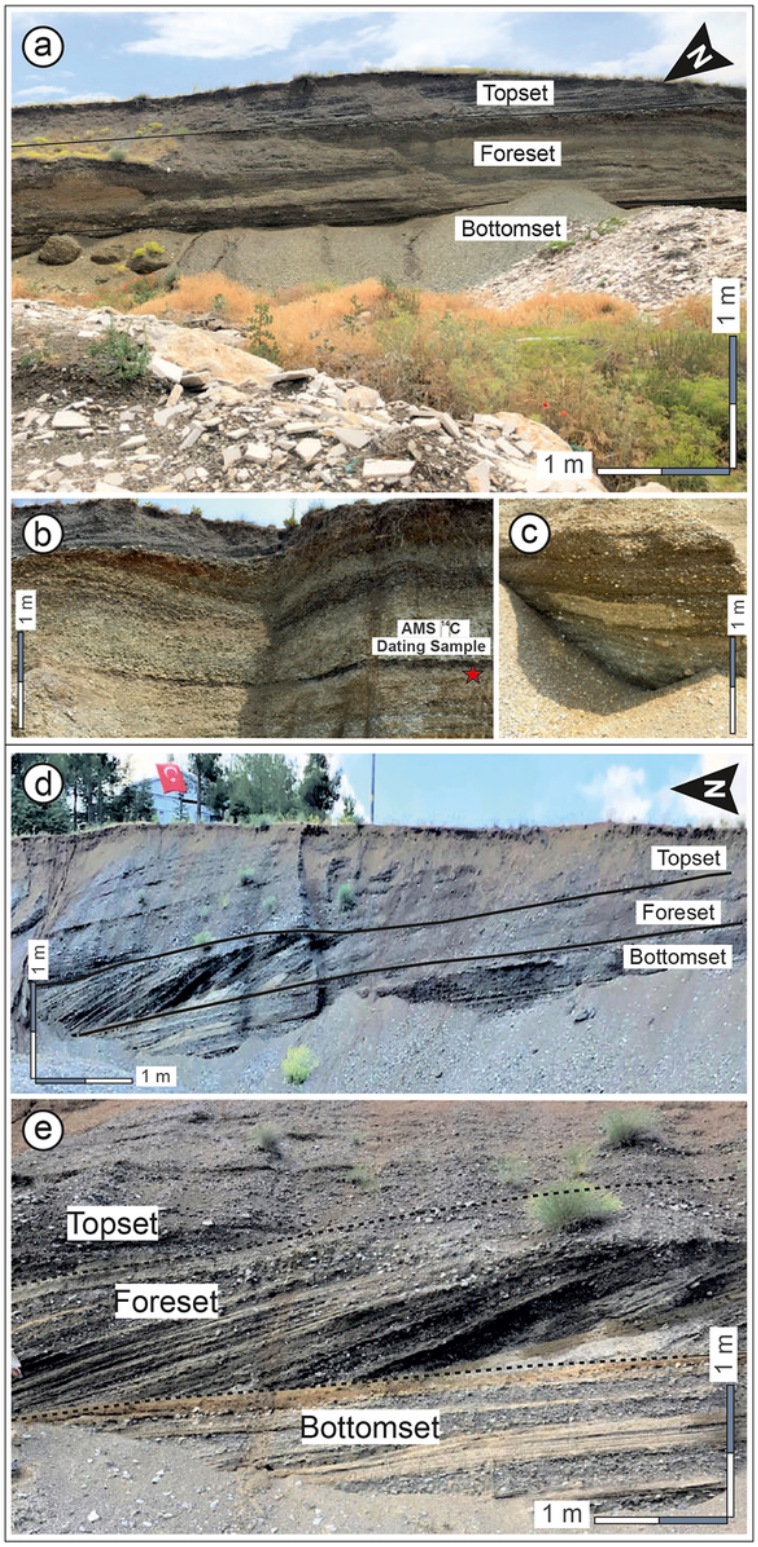

Figure 2

Raw data of NE-SW oriented high-resolution seismic profile SLD-01 at the top, showing location of core Salda2014-P02. **(a)** The main seismic facies configurations of units S4 to S1 in the inner shelf and **(b)** and **(c)** in the outer shelf. Core Salda2014-P02 penetrates unit S3 in the seismic profile. Unit S4 is truncated by the reflection surface SR-3, over which unit S3 is deposited with lakeward dipping internal

reflectors **(c).** Unit S2 is represented by moderate to strong sub-horizontal internal reflectors with coastal onlaps **(b)**.

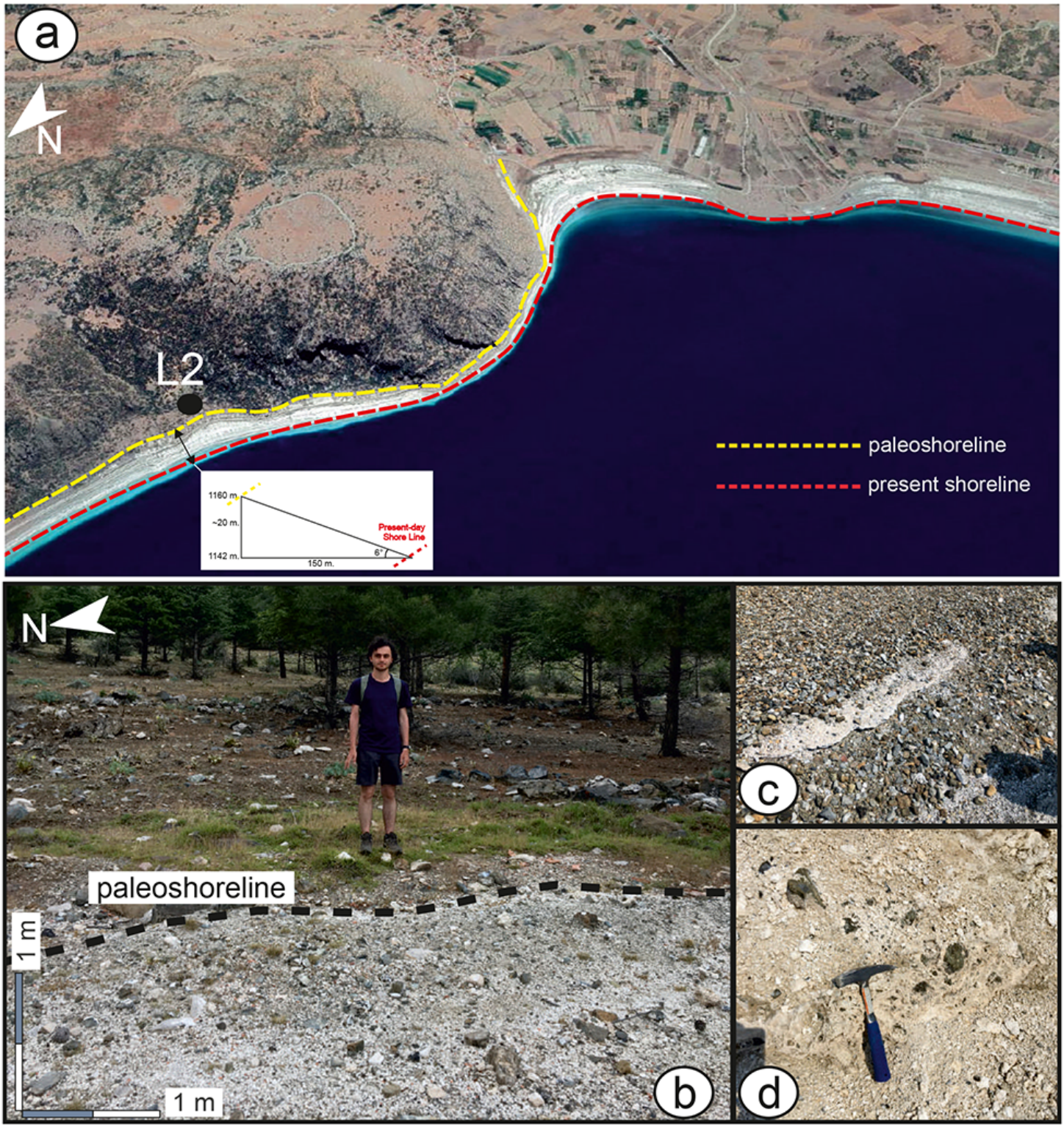

Figure 3

(a) Raw data (upper) and interpretation (lower) of NE-SW oriented high-resolution seismic profile SLD-05, showing the main seismic facies configurations of units S4 to S1. Unit S4 is truncated by the reflection surface SR-3, over which unit S3 is deposited with prograding clinoforms. Unit S2 is represented by moderate to strong sub-horizontal internal reflectors with coastal onlaps. **(b)** Raw data (upper) and interpretation (lower) of NE-SW oriented high-resolution seismic profile SLD-11, showing the main seismic facies configurations of units S3 to S1. In this profile, the formation of a stromatolite (unit S3) above the acoustic basement is marked by mounded morphology. In the profile, the wedge-shaped lenticular channel-fills of unit S2 overlies reflection surface SR-2 that implies channel-incisions.

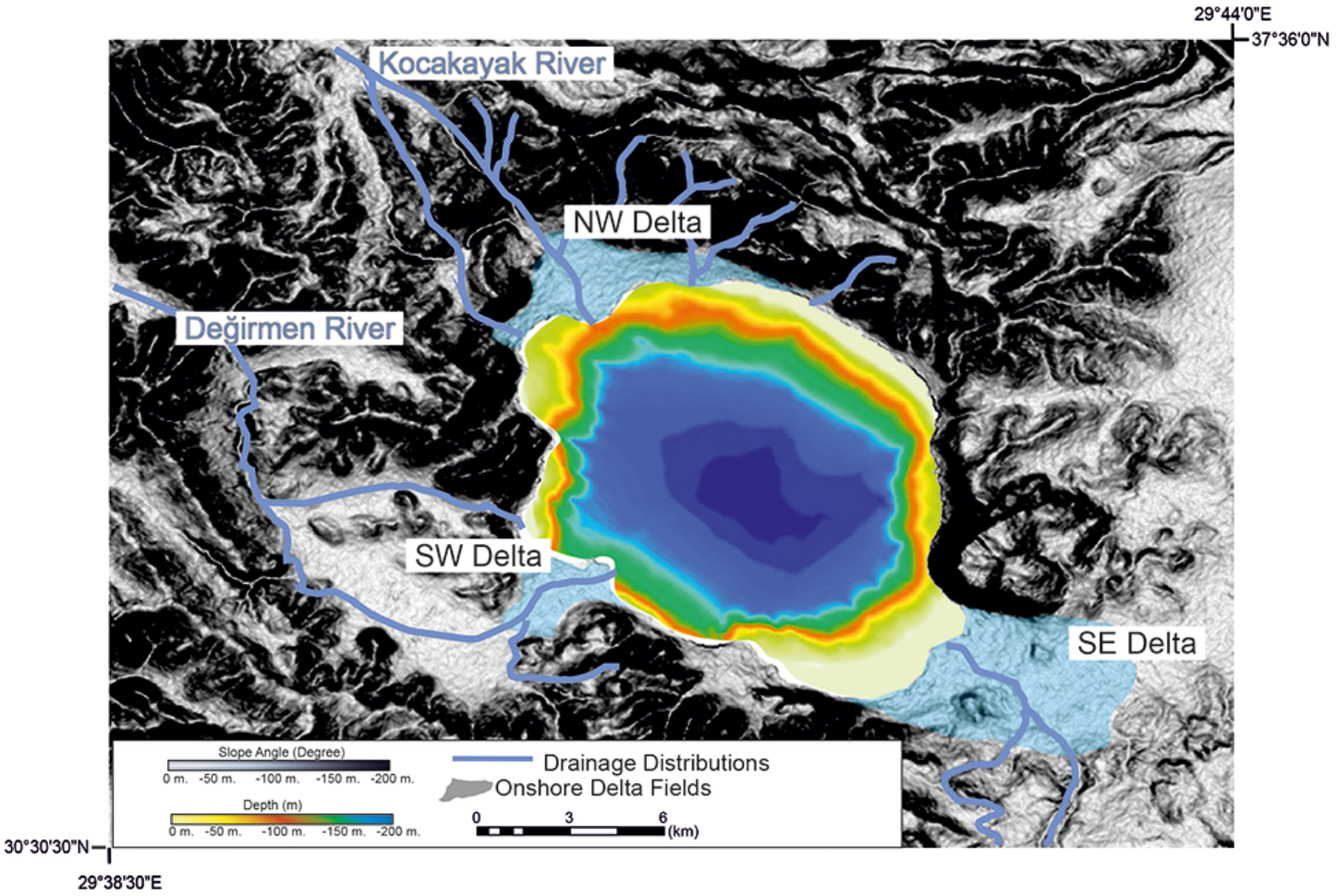

Figure 4

Raw data (upper) and interpretation (lower) of SW-NE oriented high-resolution seismic profile SLD-07 at the top shows the location of core Salda-2. The main seismic facies configurations indicate two discrete deltaic complexes of units S3 (older) and S2 (younger), implying delta retreat in the inner shelf of the lake. Core Salda-2 penetrates the uppermost of unit S3 that is the lakeward equivalence of the older deltaic sediment.

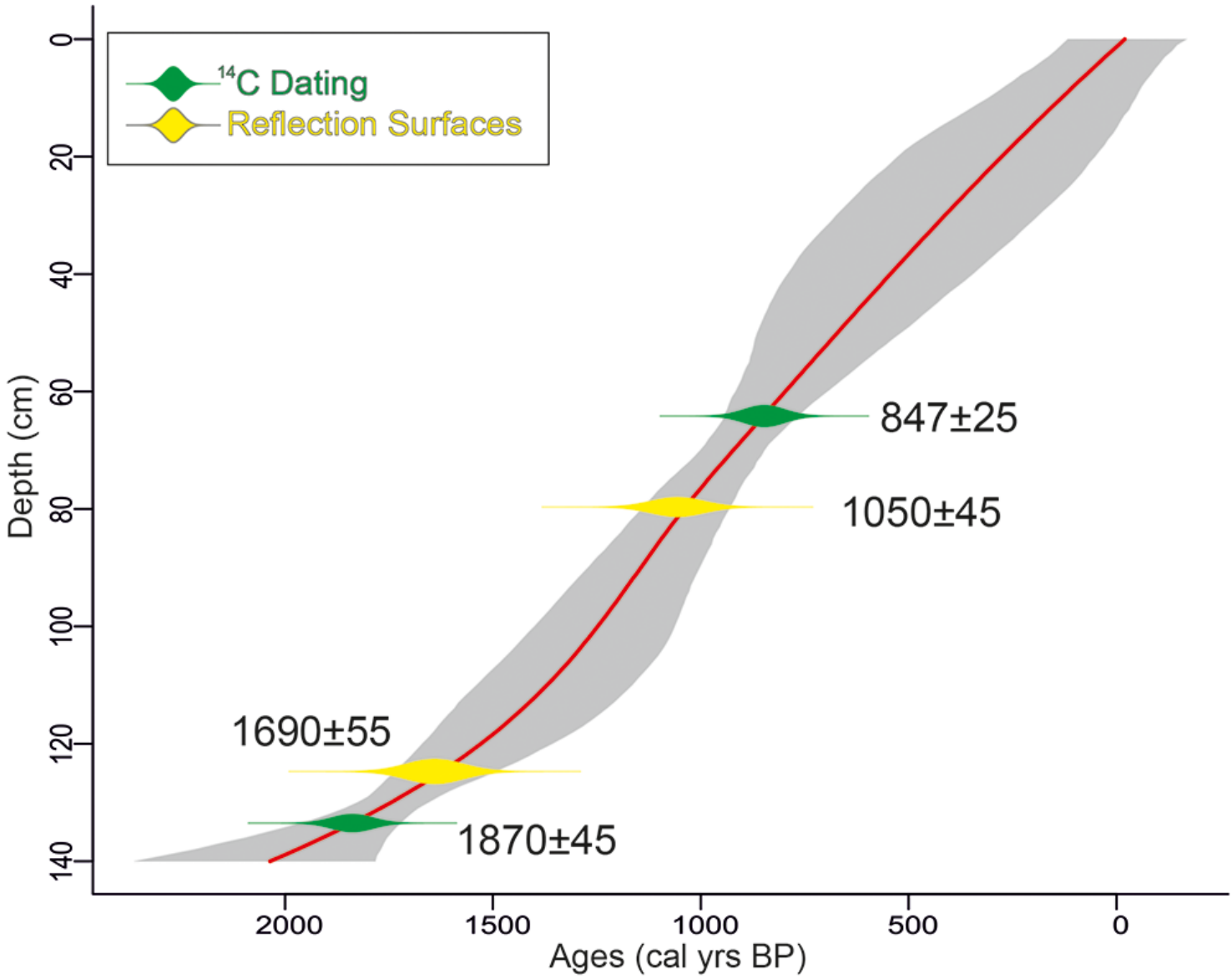

Figure 5

Lithostratigraphic subdivisions of the studied cores Salda2014-P02 and Salda-2 based on the lithologic and textural variations, showing the late Holocene sedimentary units deposited in Lake Salda (for locations of cores, see Fig. 1).

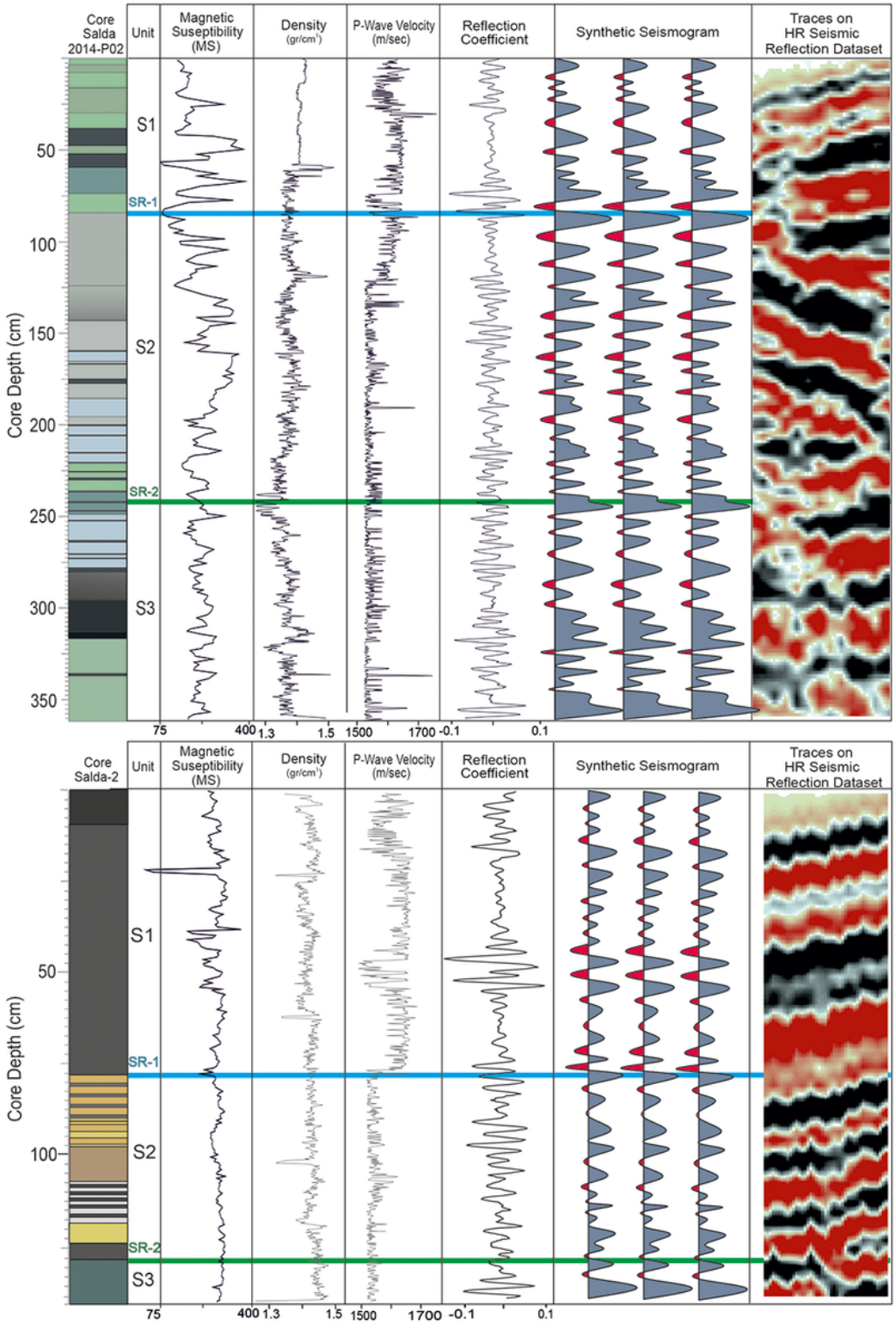

Figure 6

Synthetic seismograms (two-way travel time (TWTT) domain in millisecond) of the studied cores based on MSCL analyses, providing precise matchings between lithostratigraphic and seismic stratigraphic units defined in the studied cores and seismic profiles SLD-01 and SLD-07. According to the synthetic seismograms, the remarkable reflection surfaces (SR-1 and SR-2) in the seismic profiles coincide with sudden variations in the density and P-wave profiles of the cores.

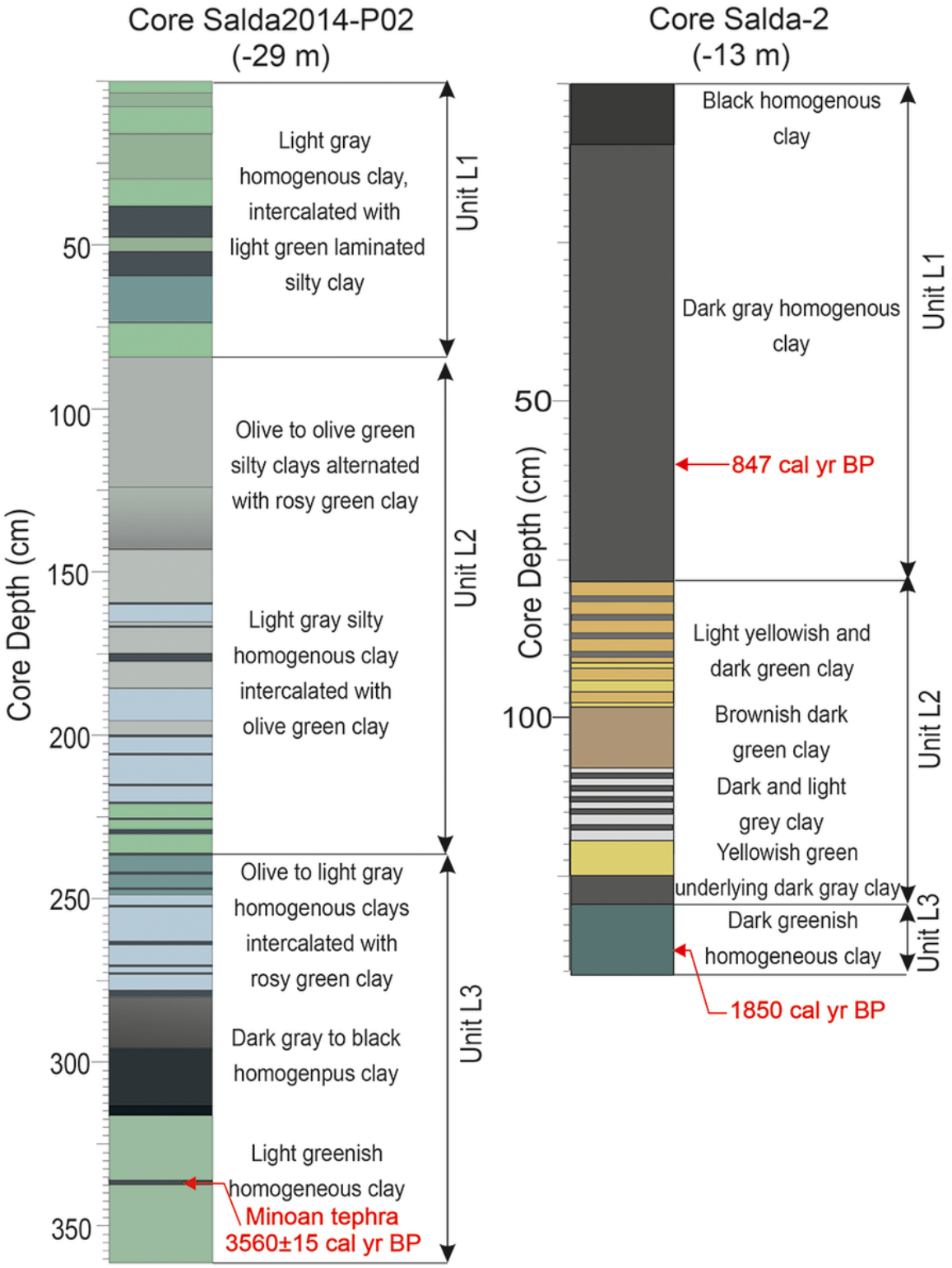

Figure 7

Age-depth model of sediment core Salda-2 based on AMS ^{14}C ages by using Bacon.r Script. Red line represents the mean age of the iteration. Green dots represent ^{14}C AMS datings. Core to seismic correlations based on synthetic seismograms allow us to estimate ages of seismic reflection surfaces

SR-1 and SR-2 shown as yellow dots in this figure. Grayscale background indicates the iteration of distribution.

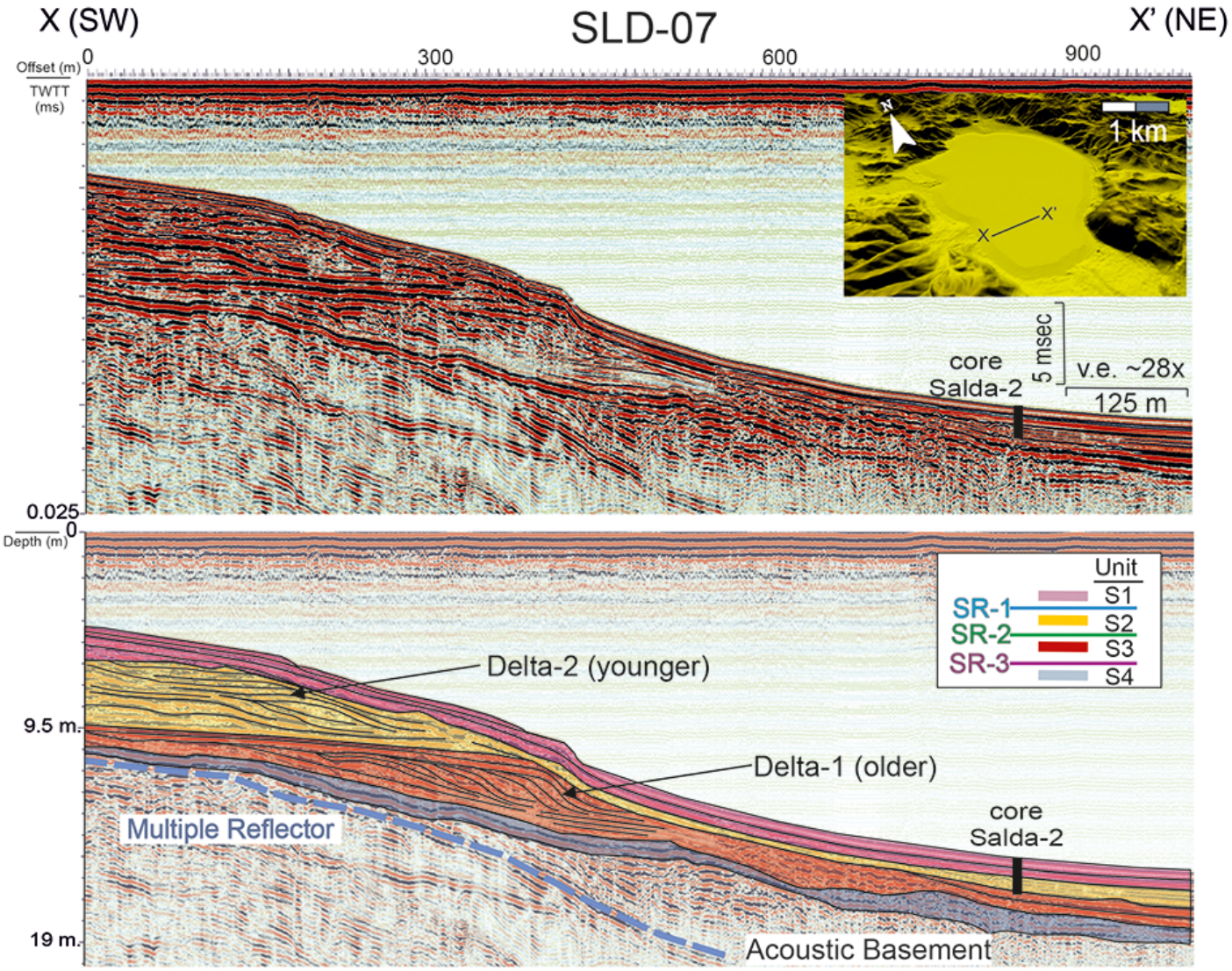

Figure 8

A relief map around Lake Salda produced from DEM datasets shows the main drainage networks on the catchment area and present delta plains around the lake. The figure also shows interpolated general lake bathymetry based on the HR seismic data. The bathymetric depths (meters) are represented by different colors.

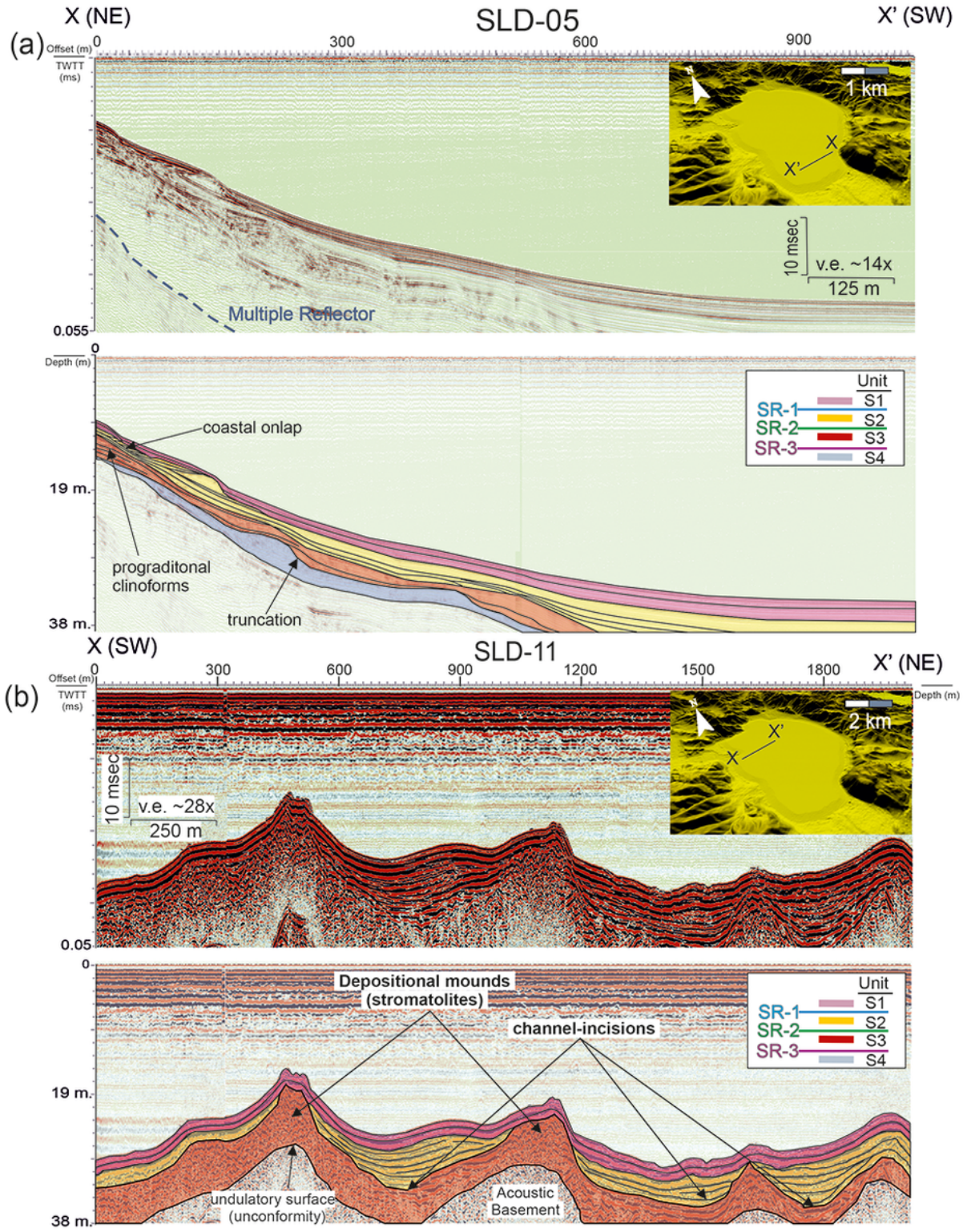

Figure 9

a) Google Earth image from NE sector of lake coastline showing location (black dot) of the lake terrace above ~22 m from present lake level and its trace along the coastline. **b)** outcrop picture showing the latest Holocene lake terrace. (**c and d**) detailed lithology and texture of paleoshoreline deposits, comprising beige color clayey hydromagnesite sand with well-rounded pebbles.

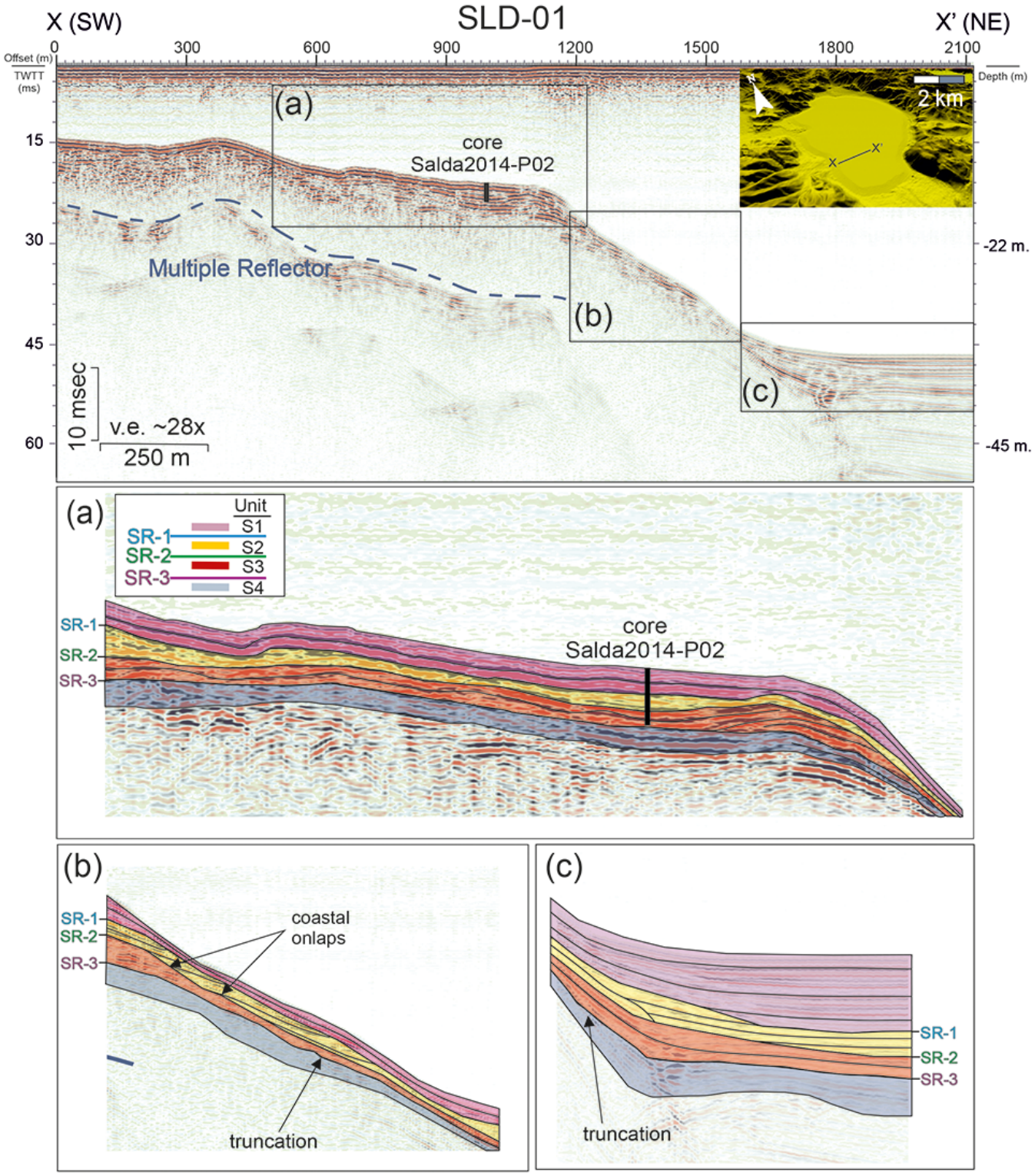

Figure 10

a) (1) The outcrop picture of the eastern deltaic-complex (location L-1 in Fig.1), showing bottomset, foreset and topset beds. **b)** detailed lithology and texture of the topset of the deltaic and AMS ^{14}C dating (red star) obtained from a peat layer, giving an age younger than 700 year BP. **c)** detailed lithology and texture of the bottomset of the delta. **d)** The outcrop picture of the western deltaic-complex (location L-3 in Fig.1). **e)** outcrop picture of the deltaic deposits, showing bottomset, foreset and topset beds.

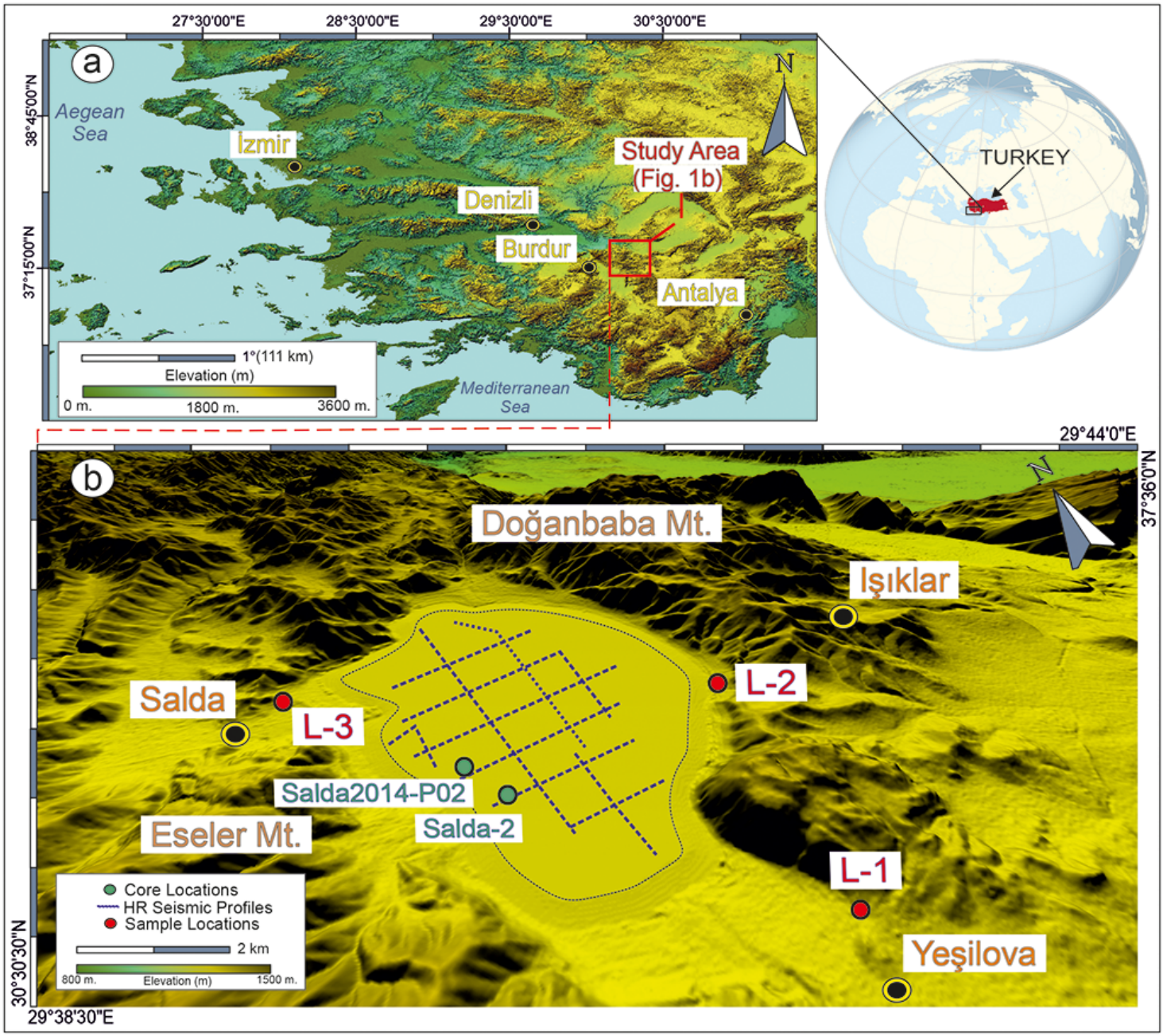

Figure 11

Synthetic seismogram and reflection coefficient sourced regression model in sediment core Salda-2 on age/time domain. Red line graph indicates the calculated sedimentation rate based on the age-depth model of the core. The figure also shows relative lake level variations during the deposition of seismic stratigraphic units in the lake during the late Holocene.